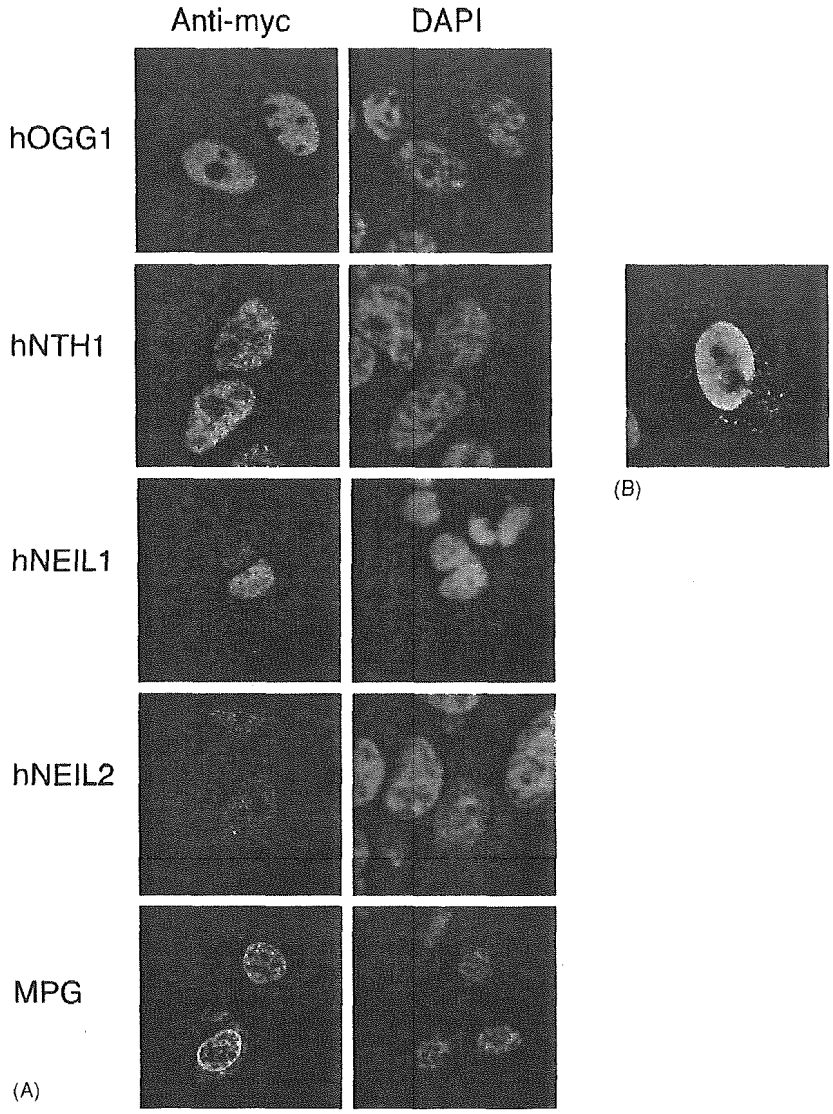

Fig. 4. (A) Subcellular localisation of hOGG1, hNTH1, hNEIL1, hNEIL2 and MPG in HeLa cells. Constructs containing the myc-tagged proteins were transfected in HeLa cells and cells were fixed and immunolabeled with anti-myc antibody (first column). Nuclear DNA was counterstained with DAPI (second column); (B) hNTH was localised in the mitochondria in about 10% of the cells.

capacity to modulate several of the enzymatic activities, a handing off model was proposed in which XRCC1 coordinates the processing of the damaged DNA [17,18]. The results presented here generalize this coordinating role of XRCC1 to all the steps involved in the repair of oxidised pyrimidines and alkylated bases.

By its interactions with DNA glycosylases, XRCC1 would be recruited to the BER process right after recognition of the lesion and accompany the DNA during the whole progression of repair, a model supported by recent in vivo kinetics experiments suggesting the involvement of XRCC1 in the repair of oxidised bases [28]. In this model, DNA is passed from one complex to the next. The efficient handing off of the substrate between the different XRCC1 complexes is facilitated by the properties of this protein. The weak and/or transient nature of the XRCC1 interactions with the enzymes (with the exception of LIG3 for which XRCC1 plays also a stabilizing role) allows a dynamic assembly and disassembly of the complexes, switching from one partner to the other according to the kind of damage or repair intermediate being processed. Furthermore, its capacity to bind DNA [29,30] suggests the possibility that XRCC1 could also hold the DNA during the transactions. The modular organisation of the XRCC1 domains is particularly fitted to its scaffolding function. The separated and distinct binding domains allow the presence of two or more enzymes docked to XRCC1, potentially allowing the hand off of the DNA to occur in complexes harbouring two sequential enzymes associated by XRCC1. It is interesting to note that OGG1 [15], APE1 [14] and PARP1 [7], all three enzymes initiators for the repair of 8-oxoG, AP sites and single-strand breaks, respectively, bind the same region of XRCC1, namely the one spanning the first linker and the

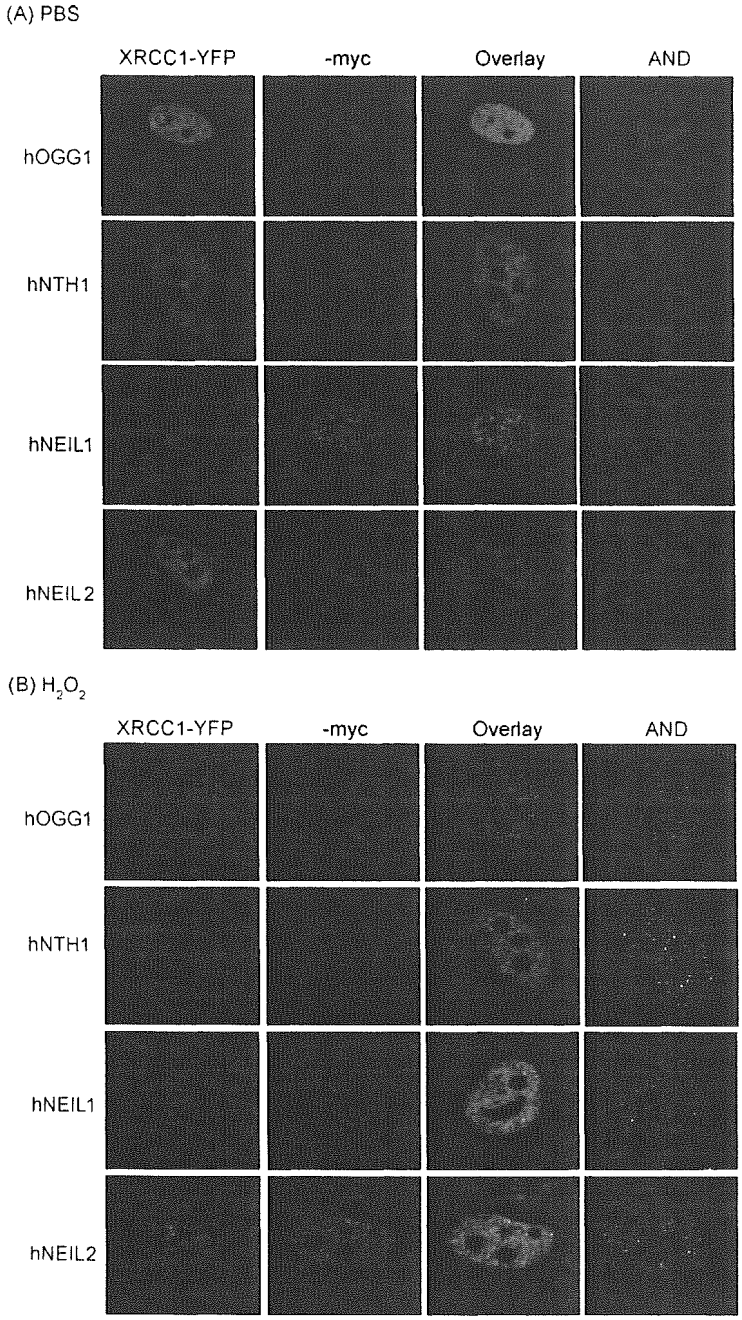

Fig. 5. Co-localization of XRCC1 and DNA glycosylases hOGG1, hNTH1, hNEIL1 and hNEIL2. HeLa cells were transfected with plasmids expressing XRCC1-YFP and the myc-tagged DNA glycosylases. Cells were treated for 30 min with PBS or 5 mM H_2O_2 in PBS, washed and incubated in DMEM medium for 1 h prior to fixation and immunostaining with anti-myc antibody. The AND images were obtained with the MetaMorph software as described in Section 2 and represent the foci where both proteins co-localise.

BRCT1. Here, we have confirmed this observation by showing that the same domain is involved in the binding to NEIL2 and NTH. These results suggest that XRCC1 is recruited to the repair through a common mechanism involving the linker and BRCT1 for different DNA lesions. In the case of modified bases, depending on the kind of reaction catalysed by the DNA glycosylase two scenarios can be proposed. If the DNA glycosylase is monofunctional or a member of the *Endo*III family, the product of the reaction can be either an AP site or a nick with a 3′-open aldehyde. In both cases APE1 is recruited to generate a 3′-OH. Alternatively, it has been recently proposed that an oxidised pyrimidine or an AP site could be a NEIL1 substrate to yield a gap with framed by both 3′- and 5′-phosphates and the repair could be continued by the recruitment of PNK and independently of APE1 [16]. Interestingly, the same authors showed a NEIL1–XRCC1 interaction. Our

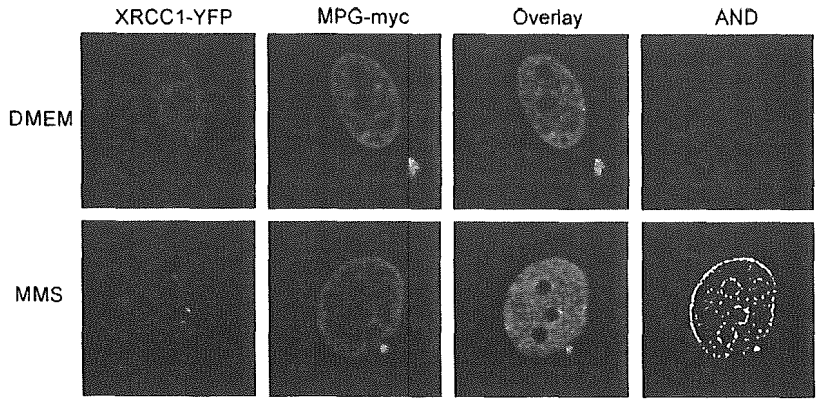

Fig. 6. Co-localization of XRCC1 and the MPG glycosylase. HeLa cells were transfected with plasmids expressing XRCC1-YFP and the myc-tagged MPG. Cells were treated for 20 min with or without 10 μg/ml MMS in DMEM, washed and incubated in DMEM medium for 1 h prior to fixation and immunostaining with the anti-myc antibody. The AND images are as in Fig. 5.

results suggest that a similar situation is possible in the case of NEIL2. In both scenarios, the enzyme following the DNA glycosylase, APE1 or PNK, is recruited by XRCC1.

Taken together, the results presented here support a unifying model by which XRCC1 would be recruited to the site of the lesion, either a modified base, an AP site or a SSB, through the interaction of its linker-BRCT1 region with the enzymes initiating BER or SSBR. This opens the question about what mechanisms result in an increased affinity of XRCC1 for the repair enzymes. The recent findings that some of the glycosylases interacting with XRCC1 are susceptible of post-translational modifications [31,32] and that XRCC1 can also be phosphorylated [33], could provide one explanation for the dynamic assembly or disassembly of the described XRCC1 complexes. Alternatively, conformational changes in the enzymes upon their interaction with the damaged DNA could increase their affinity for XRCC1.

Acknowledgements

We would like to thank the staff of the Plate-Forme Imagerie et Biologie Cellulaire, CNRS, Gif sur Yvette, for their help with confocal microscopy. We are grateful to Dr. Daisuke Tsuchimoto for his comments on the manuscript and together with Dr. Kumiko Torisu for their confirmation of DNA sequence of Neil 1 and 2 cDNAs. This work was supported by the Association pour la Recherche sur le Cancer (ARC 4688), Electricité de France (EDF) and EC grant FIGH-CT 2002-0027.

References

[1] T. Lindahl, Instability and decay of the primary structure of DNA, Nature 362 (1993) 709–715.
[2] T. Lindahl, R.D. Wood, Quality control by DNA repair, Science 286 (1999) 1897–1905.
[3] K.W. Caldecott, XRCC1 and DNA strand break repair, DNA Repair (Amst) 2 (2003) 955–969.
[4] S. Okano, L. Lan, K.W. Caldecott, T. Mori, A. Yasui, Spatial and temporal cellular responses to single-strand breaks in human cells, Mol. Cell Biol. 23 (2003) 3974–3981.
[5] S.F. El-Khamisy, M. Masutani, H. Suzuki, K.W. Caldecott, A requirement for PARP-1 for the assembly or stability of XRCC1 nuclear foci at sites of oxidative DNA damage, Nucleic Acids Res. 31 (2003) 5526–5533.
[6] K.W. Caldecott, S. Aoufouchi, P. Johnson, S. Shall, XRCC1 polypeptide interacts with DNA polymerase beta and possibly poly (ADP-ribose) polymerase, and DNA ligase III is a novel molecular 'nick-sensor' in vitro, Nucleic Acids Res. 24 (1996) 4387–4394.
[7] M. Masson, C. Niedergang, V. Schreiber, S. Muller, J. Menissier-de Murcia, G. de Murcia, XRCC1 is specifically associated with Poly(ADP-Ribose) polymerase and negatively regulates its activity following DNA damage, Mol. Cell Biol. 18 (1998) 3563–3571.
[8] V. Schreiber, J.C. Ame, P. Dolle, I. Schultz, B. Rinaldi, V. Fraulob, J. Menissier-de Murcia, G. de Murcia, Poly(ADP-ribose) polymerase-2 (PARP-2) is required for efficient base excision DNA repair in association with PARP-1 and XRCC1, J. Biol. Chem. 277 (2002) 23028–23036.
[9] Y. Kubota, R.A. Nash, A. Klungland, P. Schar, D.E. Barnes, T. Lindahl, Reconstitution of DNA base excision-repair with purified human proteins: interaction between DNA polymerase beta and the XRCC1 protein, EMBO J. 15 (1996) 6662–6670.
[10] Dianova II, K.M. Sleeth, S.L. Allinson, J.L. Parsons, C. Breslin, K.W. Caldecott, G.L. Dianov, XRCC1-DNA polymerase beta interaction is required for efficient base excision repair, Nucleic Acids Res. 32 (2004) 2550–2555.
[11] K.W. Caldecott, C.K. McKeown, J.D. Tucker, S. Ljungquist, L.H. Thompson, An interaction between the mammalian DNA repair protein XRCC1 and DNA ligase III, Mol. Cell Biol. 14 (1994) 68–76.
[12] C.J. Whitehouse, R.M. Taylor, A. Thistlethwaite, H. Zhang, F. Karimi-Busheri, D.D. Lasko, M. Weinfeld, K.W. Caldecott, XRCC1 stimulates human polynucleotide kinase activity at damaged DNA termini and accelerates DNA single-strand break repair, Cell 104 (2001) 107–117.
[13] I. Plo, Z.Y. Liao, J.M. Barcelo, G. Kohlhagen, K.W. Caldecott, M. Weinfeld, Y. Pommier, Association of XRCC1 and tyrosyl DNA phosphodiesterase (Tdp1) for the repair of topoisomerase I-mediated DNA lesions, DNA Repair (Amst) 2 (2003) 1087–1100.
[14] A.E. Vidal, S. Boiteux, I.D. Hickson, J.P. Radicella, XRCC1 coordinates the initial and late stages of DNA abasic site repair through protein–protein interactions, EMBO J. 20 (2001) 6530–6539.
[15] S. Marsin, A.E. Vidal, M. Sossou, J. Menissier-de Murcia, F. Le Page, S. Boiteux, G. de Murcia, J.P. Radicella, Role of XRCC1 in the coordination and stimulation of oxidative DNA damage repair

initiated by the DNA glycosylase hOGG1, J. Biol. Chem. 278 (2003) 44068–44074.
[16] L. Wiederhold, J.B. Leppard, P. Kedar, F. Karimi-Busheri, A. Rasouli-Nia, M. Weinfeld, A.E. Tomkinson, T. Izumi, R. Prasad, S.H. Wilson, S. Mitra, T.K. Hazra, AP endonuclease-independent DNA base excision repair in human cells, Mol. Cells 15 (2004) 209–220.
[17] P.A. Rice, Holding damaged DNA together, Nat. Struct. Biol. 6 (1999) 805–806.
[18] S.H. Wilson, T.A. Kunkel, Passing the baton in base excision repair, Nat. Struct. Biol. 7 (2000) 176–178.
[19] M. Audebert, J.P. Radicella, M. Dizdaroglu, Effect of single mutations in the OGG1 gene found in human tumors on the substrate specificity of the OGG1 protein, Nucleic Acids Res. 28 (2000) 2672–2678.
[20] T.R. O'Connor, Purification and characterization of human 3-methyladenine-DNA glycosylase, Nucleic Acids Res. 21 (1993) 5561–5569.
[21] T. Izumi, L.R. Wiederhold, G. Roy, R. Roy, A. Jaiswal, K.K. Bhakat, S. Mitra, T.K. Hazra, Mammalian DNA base excision repair proteins: their interactions and role in repair of oxidative DNA damage, Toxicology 193 (2003) 43–65.
[22] M. Audebert, J.B. Charbonnier, S. Boiteux, J.P. Radicella, Mitochondrial targeting of human 8-oxoguanine DNA glycosylase hOGG1 is impaired by a somatic mutation found in kidney cancer, DNA Repair (Amst) 1 (2002) 497–505.
[23] S. Boiteux, J.P. Radicella, The human OGG1 gene: structure, functions, and its implication in the process of carcinogenesis, Arch. Biochem. Biophys. 377 (2000) 1–8.
[24] R. Aspinwall, D.G. Rothwell, T. Roldan-Arjona, C. Anselmino, C.J. Ward, J.P. Cheadle, J.R. Sampson, T. Lindahl, P.C. Harris, I.D. Hickson, Cloning and characterization of a functional human homolog of *Escherichia coli* endonuclease III, Proc. Natl. Acad Sci. U.S.A. 94 (1997) 109–114.
[25] M. Takao, S. Kanno, K. Kobayashi, Q.M. Zhang, S. Yonei, G.T. van der Horst, A. Yasui, A back-up glycosylase in Nth1 knock-out mice is a functional Nei (endonuclease VIII) homologue, J. Biol. Chem. 277 (2002) 42205–42213.
[26] M.E. Stauffer, W.J. Chazin, Structural mechanisms of DNA replication, repair, and recombination, J. Biol. Chem. 279 (2004) 30915–30918.
[27] L.H. Thompson, M.G. West, XRCC1 keeps DNA from getting stranded, Mutat. Res. 459 (2000) 1–18.
[28] L. Lan, S. Nakajima, Y. Oohata, M. Takao, S. Okano, M. Masutani, S.H. Wilson, A. Yasui, In situ analysis of repair processes for oxidative DNA damage in mammalian cells, Proc. Natl. Acad. Sci. U.S.A. 101 (2004) 13738–13743.
[29] A. Marintchev, M.A. Mullen, M.W. Maciejewski, B. Pan, M.R. Gryk, G.P. Mullen, Solution structure of the single-strand break repair protein XRCC1 N-terminal domain, Nat. Struct. Biol. 6 (1999) 884–893.
[30] R.S. Mani, F. Karimi-Busheri, M. Fanta, K.W. Caldecott, C.E. Cass, M. Weinfeld, Biophysical characterization of human XRCC1 and its binding to damaged and undamaged DNA, Biochemistry 43 (2004) 16505–16514.
[31] F. Dantzer, L. Luna, M. Bjoras, E. Seeberg, Human OGG1 undergoes serine phosphorylation and associates with the nuclear matrix and mitotic chromatin in vivo, Nucleic Acids Res. 30 (2002) 2349–2357.
[32] K.K. Bhakat, T.K. Hazra, S. Mitra, Acetylation of the human DNA glycosylase NEIL2 and inhibition of its activity, Nucleic Acids Res. 32 (2004) 3033–3039.
[33] J.I. Loizou, S.F. El-Khamisy, A. Zlatanou, D.J. Moore, D.W. Chan, J. Qin, S. Sarno, F. Meggio, L.A. Pinna, K.W. Caldecott, The protein kinase CK2 facilitates repair of chromosomal DNA single-strand breaks, Cell 117 (2004) 17–28.

Priority Report

8-Oxoguanine Formation Induced by Chronic UVB Exposure Makes *Ogg1* Knockout Mice Susceptible to Skin Carcinogenesis

Makoto Kunisada,[1] Kunihiko Sakumi,[2] Yohei Tominaga,[2] Arief Budiyanto,[1] Masato Ueda,[1] Masamitsu Ichihashi,[1] Yusaku Nakabeppu,[2] and Chikako Nishigori[1]

[1]Division of Dermatology, Clinical Molecular Medicine, Faculty of Medicine, Kobe University Graduate School of Medicine, Kobe, Japan and [2]Division of Neurofunctional Genomics, Medical Institute of Bioregulation, Kyusyu University, Fukuoka, Japan

Abstract

Q2 **8-Oxoguanine is one of the oxidative DNA damages that can result in stable mutations. The *Ogg1* gene encodes the repair enzyme 8-oxoguanine-DNA glycosylase, which removes the oxidized base from DNA. In this study, we investigated the role of 8-oxoguanine in skin carcinogenesis induced by UVB irradiation using *Ogg1* knockout mice (C57Bl/6J background). We examined the effect of UVB irradiation on the formation of 8-oxoguanine in epidermal cells using immunostaining and found that the level of 8-oxoguanine in *Ogg1* knockout mice 24 hours after UVB irradiation remained high compared with that in wild-type and heterozygous mice. To verify the effect of chronic UVB irradiation on 8-oxoguanine formations in epidermal cells, we irradiated wild-type, heterozygous, and *Ogg1* knockout mice with UVB at a dose of 2.5 kJ/m^2 thrice a week for 40 weeks. We found that the mean number of tumors in *Ogg1* knockout mice was 3.71, which was significantly more than in wild-type and heterozygous mice, being 1.71 and 2.28, respectively. The rate of developing malignant tumors in *Ogg1* knockout mice was also significantly higher (88.5%; squamous cell carcinomas, 73.1%; sarcomas, 15.4%) than in wild-type mice (50.0%; squamous cell carcinomas, 41.7%; sarcomas, 8.3%). Moreover, the age of onset of developing skin tumors in *Ogg1* knockout mice was earlier than in the other types of mice. These results clearly indicate that oxidative DNA damage induced by sunlight plays an important role in the development of skin cancers.** (Cancer Res 2005; 65(14): 1-5)

Introduction

Reactive oxygen species, which are generated endogenously by cellular oxygen metabolism or exogenously by ionizing radiation, environmental mutagens, and carcinogens, produce various types of DNA damage. Among many oxidative DNA base modifications, 8-oxoguanine pairs with adenine as well as cytosine during DNA replication, which results in GC→TA transversion mutations (1, 2). In mammalian cells, *Ogg1* encodes a DNA glycosylase/AP lyase, which functions in the removal of 8-oxoguanine from DNA (3). Solar UV, particularly UVB (wavelength range, 280-320 nm), has been recognized to be responsible for the development of skin cancers in humans and in other animals (4). The mechanism of sunlight-related skin carcinogenesis has been extensively investigated and UV-induced pyrimidine photoproducts are thought to be a major cause of skin cancer (5, 6). UV and visible light, on the other hand, are also known to induce reactive oxygen species, and increases in 8-oxoguanine were shown in cells after UVB or visible light exposure (7, 8). In this study, we showed that *Ogg1* knockout mice are impaired in the removal of 8-oxoguanine from DNA in epidermal cells after UVB exposure and that *Ogg1* knockout mice produce significantly higher numbers of skin tumors after chronic UVB irradiation than do wild-type or heterozygous mice. In addition, we found that the ratio and incidence of malignant skin tumors produced by chronic UVB irradiation in *Ogg1* knockout mice were significantly higher and occurred at an earlier age than in wild-type or heterozygous mice. Although there are several reports about the association between the inactivation of *Ogg1* and cancer risk (9–11), this study directly clarifies the importance of oxidative DNA damage caused by UVB irradiation in developing skin cancers using *Ogg1* knockout mice.

Materials and Methods

Knockout mice. The development of *Ogg1* knockout mice has been described previously (9). We inbred *Ogg1* heterozygous mice (C57Bl/6J, N:12) and determined three *Ogg1* genotypes, wild-type, heterozygous, and knockout, using genomic PCR. The procedure used for PCR, including the position and primers used, has been previously described (9). Mice, ages 12 to 15 weeks, were selected and divided into three groups of 10 mice for *Ogg1* genotype, wild-type, heterozygous, and knockout, to be used for UV irradiation. In addition, five mice of each genotype were sham irradiated. The mice were housed under special pathogen-free conditions and all animal experiments were conducted according to the "Guideline for Animal Experimentation at Kobe University School of Medicine."

UVB irradiation. A bank of six TL 20W/12RS fluorescent lamps (Philips, Eindhoven, Holland) was used to irradiate the mice. These lamps emit a continuous spectrum from 275 to 390 nm, with a peak emission at 313 nm; ~65% of that radiation is within the UVB wavelength range. The irradiance was 3.8 J/m^2/s at a distance of 40 cm, as measured by an UVR-305/365D digital radiometer (Tokyo Kogaku Kikai KK, Tokyo, Japan). For skin tumor production, the backs of mice were shaved and the mice were placed 40 cm below the light source and irradiated with 2.5 kJ/m^2 UVB thrice per week for 40 weeks. Exposure to 2.5 kJ/m^2 is an approximate subminimal erythema dose for C57Bl/6J mice. For immunohistochemical detection of 8-oxoguanine after UVB irradiation, mice of age 12 weeks were irradiated with 3.0 kJ/m^2.

Immunohistochemistry. *For detection of 8-oxoguanine in mouse skin,* skin specimens were collected 3 and 24 hours after UVB irradiation. Skin specimens were fixed in 10% neutralized formalin and embedded in paraffin. Sections were cut, deparaffinized, rehydrated, and washed in PBS. Sections were microwaved thrice in 10 mmol/L citrate buffer (pH 6.0) for 5 minutes. After blocking endogenous peroxidase, nonspecific binding sites were blocked by incubating the sections with protein blocking serum (Dako, Kyoto, Japan). Sections were incubated for 1 hour at 40°C with the primary

Requests for reprints: Chikako Nishigori, Division of Dermatology, Clinical Molecular Medicine, Faculty of Medicine, Kobe University Graduate School of Medicine, *Kobe 650-0017, Japan. Phone:* 817-838-26134; Fax: 817-838-26149; E-mail: chikako@med.kobe-u.ac.jp.

mouse monoclonal antibody against 8-oxoguanine, N45.1 (8). After washing with PBS, the sections were incubated with biotin-conjugated anti-mouse immunoglobulin G (Dako) for 20 minutes at room temperature, followed by incubation for 15 minutes with streptavidin-conjugated horseradish peroxidase (Dako) at room temperature, and finally mounted in glycergel mounting medium (Dako).

Observation and measurement of cumulative tumor incidence. After the chronic UVB exposure, we observed tumor formation until all mice developed skin tumors. The number of developing tumors with diameters larger than 2 mm was counted. Tumors <2 mm in diameter, or regressed, were not counted. The number of tumors of mice that died during the experiment was not included. All mice were sacrificed at the final observation, and all skin tumors were excised and examined histologically with H&E staining. In addition, all mice, including mice that died during the experiment, were subjected to autopsy to confirm whether they had internal spontaneous tumors macroscopically.

Histologic analysis. Biopsied tumors were fixed with 10% neutralized formalin, embedded in paraffin, and then stained using H&E. Tumors examined histologically were classified as squamous cell carcinomas (tumors with atypical epithelial differentiation), sarcomas (tumors with atypical mesenchymal differentiation), papillomas (tumors with papillomatous growth of epidermal cells without atypicality), or hemangiomas.

Statistical analysis. Statistical differences were examined with unpaired *t* test for mean number of tumors per mouse and with χ^2 test for malignant tumor rate; $P < 0.05$ is considered to be statistically significant.

Results and Discussion

8-Oxoguanine can be generated via a variety of agents such as chemicals, X-radiation, and UV and visible light in the presence of a photosensitizer, and 8-oxoguanine is accepted as a sensitive marker of oxidative DNA damage (3, 12). 8-Oxoguanine induces GC→TA transversions by mispairing with A as well as C. GC→TA transversions have been observed in the *ras* and *p53* genes in UVB-induced mice skin cancers as well as in human non-melanoma skin cancers of sun-exposed areas, which implies that 8-oxoguanine plays an important role in UV-related skin carcinogenesis (6, 13, 14). Previously it has been shown that UVB exposure increases the amount of 8-oxoguanine formations in epidermal cells (8). We examined the time course of relative amounts of 8-oxoguanine in epidermal cells of each *Ogg1* genotype immunohistochemically using monoclonal antibody against 8-oxoguanine (Fig. 1). Few cells positively stained for 8-oxoguanine F1
were seen in the epidermis of sham-irradiated skin, as expected. Skin specimens from UVB-irradiated wild-type and heterozygous mice showed similar staining patterns, where positively stained nuclei were seen 3 hours after UVB irradiation, although most of which waned to the level of sham-irradiated mice 24 hours after UVB irradiation. These data, however, are inconsistent with a

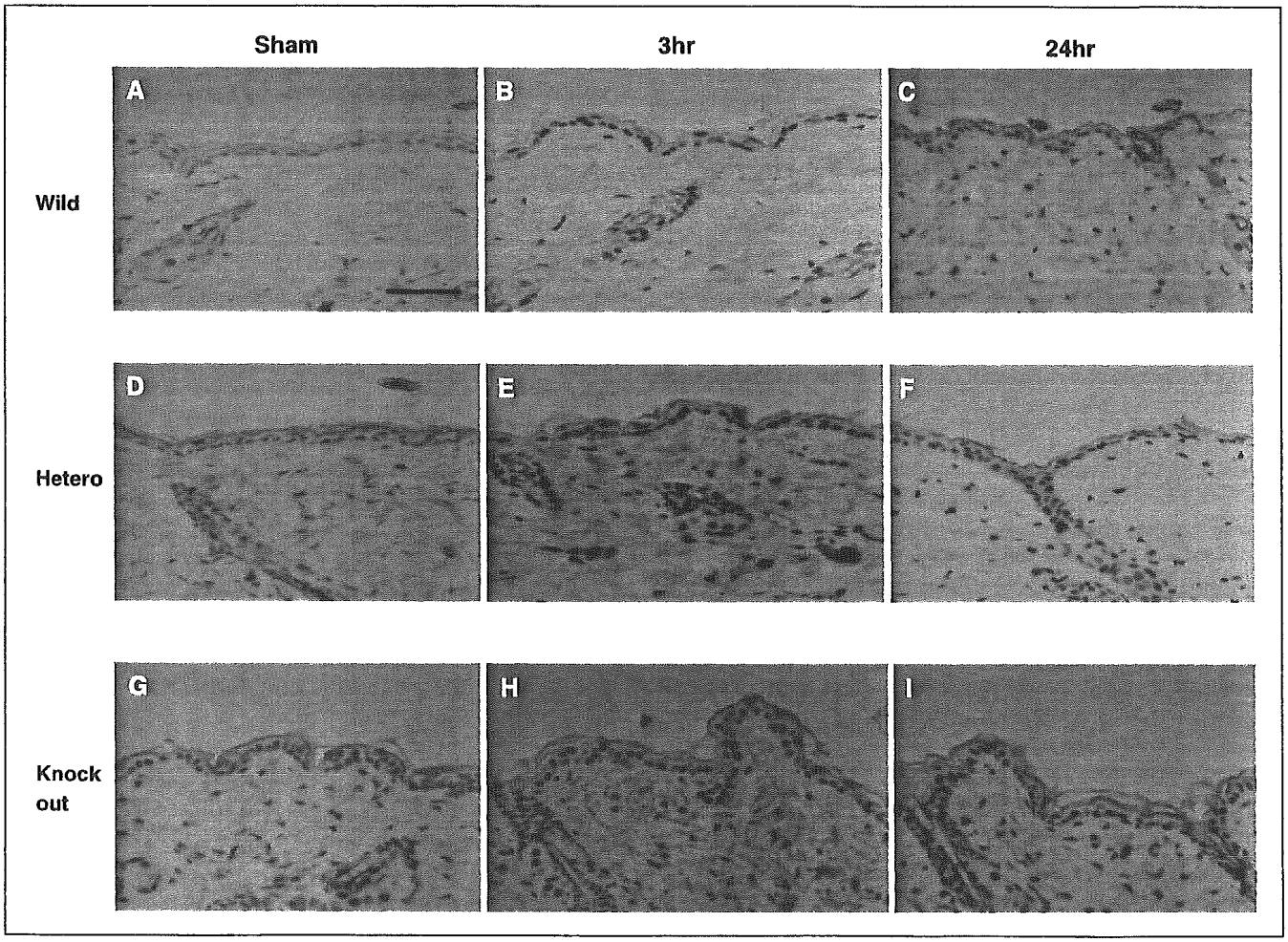

Figure 1. 8-Oxoguanine immunostaining of skin specimens from sham-irradiated (*A*, *D*, and *G*), or 3 hours (*B*, *E*, and *H*) or 24 hours (*C*, *F*, and *I*) after 3 kJ/m^2 UVB exposure of *Ogg1+/+* (*A-C*), *Ogg1+/−* (*D-F*), and *Ogg1−/−* (*G-I*) mice. Representative photomicrograph of at least three independent experiments. Bar, 100 μm.

previous report, which indicated that UV-induced 8-oxoguanine formations in hairless mouse skin were slowly removed and remained at a high level in the epidermis (12). These data with the previous reports were achieved because the dose of UVB irradiation used in this study was relatively low (subminimal erythema dose) compared with the much higher dose used in the other study, which was 10 times the minimal erythema dose (12). Yet another consideration might be that the mice used in this study were shaved hairy black mice whereas those used in the other study were albino hairless mice. Shading by the remaining hair and pigment in the skin of the mice used in this study might have reduced the direct damage to epidermal cells to some extent. Another explanation is that the difference in mice strains contributes to the variety of skin carcinogenesis, because the C57Bl background mice we studied are well known for their resistance to carcinogen (15). Consequently, the majority of 8-oxoguanine in epidermal cells of *Ogg1* heterozygous and wild-type mice was removed within 24 hours. The epidermal cells of *Ogg1* knockout mice, on the contrary, remained highly positive for 8-oxoguanine in the epidermis, even 24 hours after UVB irradiation, similar to the level observed 3 hours after UVB irradiation. This indicates that *Ogg1* knockout mice have impairment in removing 8-oxoguanine from epidermal cells. Another report showed similar results that *Ogg1* knockout mice have a decreased ability to repair 8-oxoguanine in the liver after $KBrO_3$ treatment (16). Therefore, it is reasonable to speculate that cumulative 8-oxoguanine in the skin of *Ogg1* knockout mice leads to a higher susceptibility to tumorigenesis. Indeed, we found that the mean number of tumors per mouse that developed in *Ogg1* knockout mice was significantly (2.2-fold) higher than that in wild-type mice (3.71 versus 1.71, respectively; $P < 0.01$) after 120 times UVB exposure of 2.5 kJ/m^2/time over 40 weeks (Table 1; T1 Fig. 2). The mean number of tumors per mouse for the *Ogg1* F2 knockout mice was also significantly (1.6-fold) higher than that of the heterozygous mice (3.71 versus 2.28, respectively; $P < 0.02$; Table 1). There was no significant difference between wild-type and heterozygous mice in the mean number of tumors per mouse. These findings are consistent with the 8-oxoguanine staining patterns among the three groups at 24 hours after UVB irradiation (Table 1; Fig. 1). These results show the first direct evidence that the persistent presence of 8-oxoguanine following UVB exposure is closely related to the development of skin tumors.

We did histologic analysis for all skin tumors developed. Among skin tumors produced in *Ogg1* knockout mice, 88.5% were malignant tumors (squamous cell carcinomas, 73.1%; sarcomas, 15.4%), which is a significantly higher rate than that produced in wild-type mice, in which 50.0% were malignant tumors (squamous cell carcinomas, 41.7%; sarcomas, 8.3%; $P < 0.05$; Table 1). Because there are some reports indicating that the spindle cell tumors, which appear to be sarcoma, have the characteristics of keratinocytes in terms of immunohistochemical and ultrastructural findings (17), we examined malignant tumors consisted mostly of spindle cells immunohistochemically with pan-cytokeratin and found that none of the six specimens examined showed positive staining for pan-cytokeratin (data not shown). Thus, we diagnosed these tumors as sarcoma in this study.

Furthermore, we evaluated the acceleration of developing tumors caused by *Ogg1* gene disruption. As shown in Fig. 3, F3

Ogg1 genotype	UVB irradiation	Total number of tumors			Mean number of tumors per mouse	Histological analysis (%)						
		Male	Female	Total		Malignant tumors (%)			Benign tumors (%)			Unidentified*
						Squamous cell carcinoma	Sarcoma	Total	Papilloma	Hemangioma	Total	
Wild-type	+	2 (1)†	10 (6)	12 (7)	1.71 ± 0.76‡,§	41.7 (5/12)‖	8.3 (1/12)	50.0¶ (6/12)	41.7 (5/12)	0 (0/12)	41.7 (5/12)	8.3 (1/12)
	−	0 (1)	0 (4)	0 (5)	0							
Heterozygous	+	4 (1)	12 (6)	16 (7)	2.28 ± 0.76§,**	62.5 (10/16)	6.3 (1/16)	68.8 (11/16)	25 (4/16)	6.3 (1/16)	31.3 (5/16)	0 (0/16)
	−	0 (1)	0 (4)	0 (5)	0							
Knockout	+	5 (1)	21 (6)	26 (7)	3.71 ± 1.38‡,‖	73.1 (19/26)	15.4 (4/26)	88.5† (23/26)	11.5 (3/26)	0 (0/16)	11.5 (3/26)	0 (0/16)
	−	0 (1)	0 (4)	0 (5)	0							

*Unidentified tumors were those which we were not able to make the diagnosis due to the failure of the procedure of embedding the specimens.
†The number of skin tumor–bearing mice at the end of the experiment.
‡$P < 0.01$.
§*P, not significant.*
‖The number of skin tumors/total skin tumors histologically.
¶$P < 0.05$.
**$P < 0.02$.

Ogg1 knockout mice began to develop tumors 6 and 5 weeks earlier than wild-type and heterozygous mice, respectively, and 100% incidence was reached at 41 weeks, 3 weeks earlier than in the other genotypes. The age of onset of developing tumors in *Ogg1* heterozygous mice revealed a similar pattern to the wild-type mice. Oxidative stress has been shown to be associated with multistage carcinogenesis—initiation, promotion, and progression (18). It is recognized that low levels of oxidants can modify cell-signaling proteins. Thus, it is possible that the higher rate of DNA damage accumulation in *Ogg1* knockout mice caused higher frequency of DNA mutation leading to early initiation and acceleration of tumor progression. This would explain our result showing a higher ratio of malignant tumors and earlier onset of tumor formations in *Ogg1* knockout mice compared with wild-type and heterozygous mice. Finally, after the final observation, we did autopsies of all mice, including those that died during the experiment, to confirm whether they had internal spontaneous tumors macroscopically (9), but we did not identify any evident internal tumors in any mice.

Several skin cancer–prone diseases, such as xeroderma pigmentosum, Bloom syndrome, and Werner syndrome, are known to have defects in DNA repair systems or in DNA replication systems, such as nucleotide excision repair, translesional pathway, and helicase. Repair deficiencies cause mutations, and mutations in crucial oncogene-related genes result in the development of cancers. Thus, it is reasonable that disruption of both alleles of *Ogg1* causes a skin cancer–prone phenotype (19).

We could consider another possible mechanism for the susceptibility of *Ogg1* knockout mice to skin cancers. Not only the direct attack of UVB to DNA but also the chronic inflammatory state following UV irradiation is also responsible for the formation of 8-oxoguanine (6, 8). Peroxinitrite is generated through the reaction of nitric oxide with superoxide, which is released by infiltrating neutrophils and macrophages. Reactive oxygen species derived from inflammatory cells are continuously formed. There could be another possibility that higher amount of oxidative stress accelerates epidermal hyperplasia. However, we found that there was no significant difference in the epidermal thickness among the three genotypes

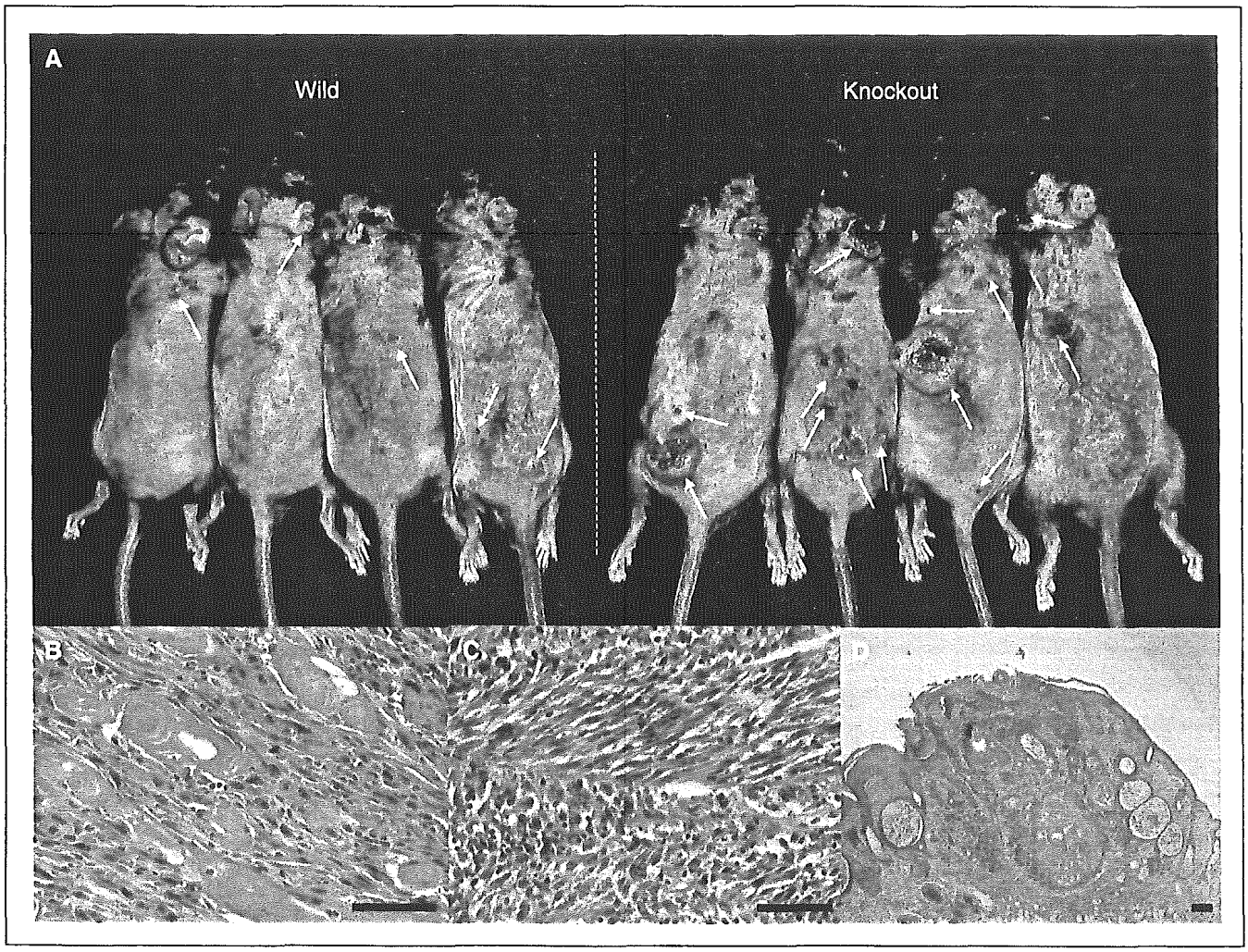

Figure 2. High susceptibility to skin carcinogenesis in *Ogg1* knockout mice. *A*, representative features of skin tumor formation in *Ogg1* wild-type mice (*left*) and in knockout mice (*right*) at the end of the observation period; arrows, developing tumors. *B*, histologic features of squamous cell carcinoma; *C*, sarcoma; *D*, papilloma stained with H&E. Bar, 100 μm.

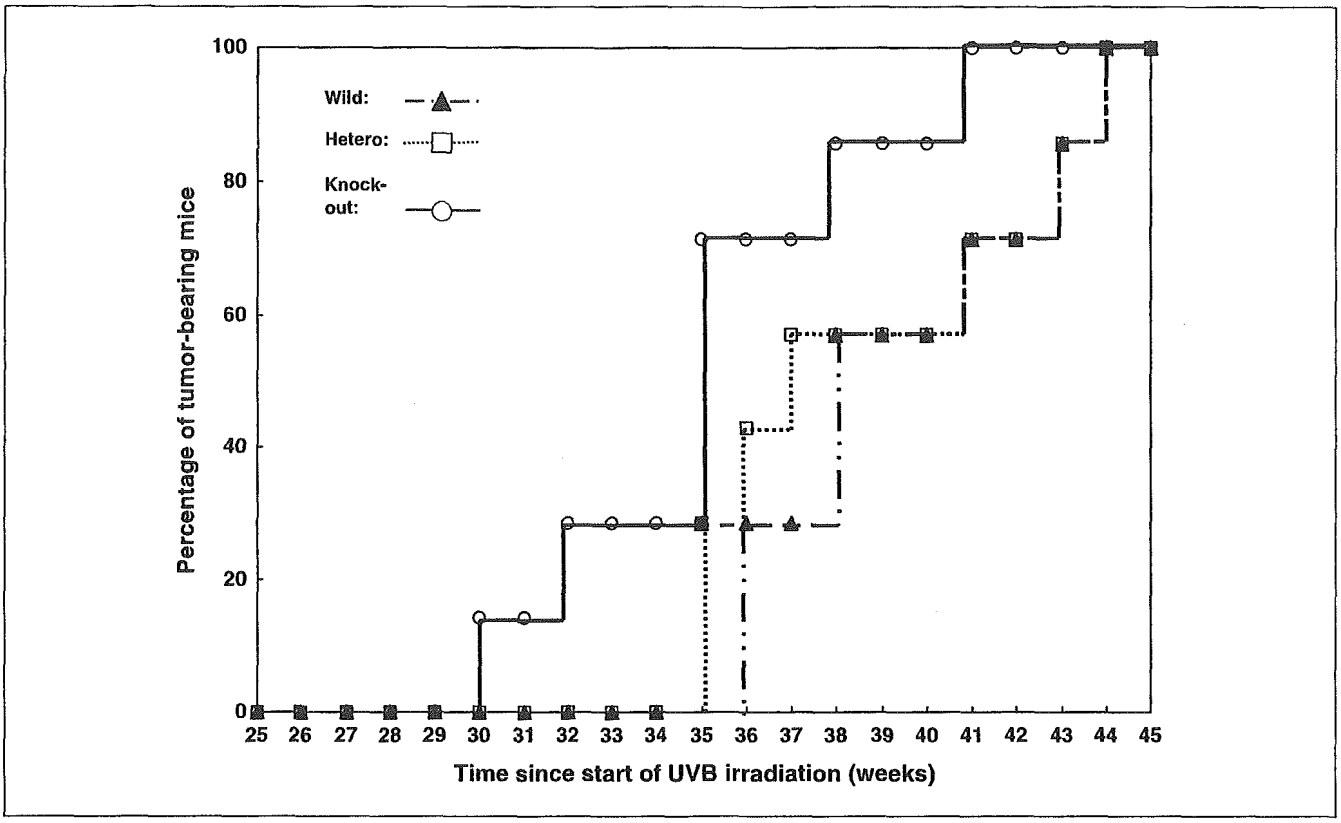

Figure 3. The effect of chronic UVB exposure on the onset and incidence of tumors in each genotype. There were 10 mice in each group at the beginning of the experiment, but only seven mice survived in each genotype group by the end of the experiment. Mice that died during the experiment were not included.

at least 24 hours after single UVB exposure, although there were subtle variations in epidermal thickness among the specimens independent of the genotype. In summary, UVB exposure generates 8-oxoguanine in epidermal cells, and *Ogg1* knockout mice have a higher susceptibility to skin cancers following chronic UVB irradiation. Oxidative DNA damage caused by UVB exposure, as well as pyrimidine photoproducts, has an important contribution in the development of skin cancers.

Acknowledgments

Received 3/2/2005; revised 5/10/2005; accepted 5/24/2005.

Grant support: Grant-in-Aid 16024211 from the Ministry of Education, Science, and Culture of Japan.

The costs of publication of this article were defrayed in part by the payment of page charges. This article must therefore be hereby marked *advertisement* in accordance with 18 U.S.C. Section 1734 solely to indicate this fact.

We thank Akemi Matsuyama and Mio Hayashi for excellent technical advice and support.

References

1. Kasai H, Chung MH, Jones DS, et al. 8-Hydroxyguanine, a DNA adduct formed by oxygen radicals: its implication on oxygen radical-involved mutagenesis/carcinogenesis. J Toxicol Sci 1991;16:95–105.
2. Maki H, Sekiguchi M. MutT protein specifically hydrolyses a potent mutagenic substrate for DNA synthesis. Nature 1992;355:273–5.
3. Aburatani H, Hippo Y, Ishida T, et al. Cloning and characterization of mammalian 8-hydroxyguanine-specific DNA glycosylase/apurinic, apyrimidinic lyase, a functional mutM homologue. Cancer Res 1997;57: 2151–6.
4. Kraemer KH. Sunlight and skin cancer: another link revealed. Proc Natl Acad Sci U S A 1997;94:11–4.
5. Drobetsky EA, Grosovsky AJ, Glickman BW. The specificity of UV-induced mutations at an endogenous locus in mammalian cells. Proc Natl Acad Sci U S A 1987;84:9103–7.
6. Nishigori C, Hattori Y, Toyokuni S. Role of reactive oxygen species in skin carcinogenesis. Antioxid Redox Signal 2004;6:561–70.
7. Yamamoto F, Nishimura S, Kasai H. Photosensitized formation of 8-hydroxydeoxyguanosine in cellular DNA by riboflavin. Biochem Biophys Res Commun 1992;187: 809–13.
8. Hattori Y, Nishigori C, Tanaka T, et al. 8-Hydroxy-2′-deoxyguanosine is increased in epidermal cells of *hairless mice after chronic ultraviolet B exposure*. J Invest Dermatol 1996;107:733–7.
9. Sakumi K, Tominaga Y, Furuichi M, et al. *Ogg1* knockout-associated lung tumorigenesis and its suppression by Mth1 gene disruption. Cancer Res 2003;63: 902–5.
10. Hardie LJ, Briggs JA, Davidson LA, et al. The effect of *hOGG1* and glutathione peroxidase I genotypes and 3p chromosomal loss on 8-hydroxydeoxyguanosine levels in lung cancer. Carcinogenesis 2000;21:167–72.
11. Xu J, Zheng SL, Turner A, et al. Associations between *hOGG1* sequence variants and prostate cancer susceptibility. Cancer Res 2002;62:2253–7.
12. Hattori-Nakakuki Y, Nishigori C, Okamoto K, Imamura S, Hiai H, Toyokuni S. Formation of 8-hydroxy-2′-deoxyguanosine in epidermis of hairless mice exposed to near-UV. Biochem Biophys Res Commun 1994;201:1132–9.
13. Nishigori C, Wang S, Miyakoshi J, et al. Mutations in *ras* genes in cells cultured from mouse skin tumors induced by ultraviolet irradiation. Proc Natl Acad Sci U S A 1994;91:7189–93.
14. Basset-Seguin N, Moles JP, Mils V, Dereure O, Guilhou JJ. *TP53* tumor suppressor gene and skin carcinogenesis. J Invest Dermatol 1994;103:102–6S.
15. Abbott PJ. Strain-specific tumorigenesis in mouse skin induced by the carcinogen, 15,16-dihydro-11-methylcyclopenta[*a*]phenanthren-17-one, and its relation to DNA adduct formation and persistence. Cancer Res 1983;43:2261–6.
16. Arai T, Kelly VP, Komoro K, Minowa O, Noda T, Nishimura S. Cell proliferation in liver of *Mmh/Ogg1*-deficient mice enhances mutation frequency because of the presence of 8-hydroxyguanine in DNA. Cancer Res 2003;63:4287–92.
17. Morrison WL, Jerdan MS, Hoover TL, Farmer ER. UV radiation-induced tumors in haired mice: identification as squamous cell carcinomas. J Natl Cancer Inst 1986;77: 1155–62.
18. Guyton KZ, Kensler TW. Oxidative mechanisms in carcinogenesis. Br Med Bull 1993;49:523–44.
19. Nishigori C, Moriwaki S, Takebe H, Tanaka T, Imamura S. Gene alterations and clinical characteristics of xeroderma pigmentosum group A patients in Japan. Arch Dermatol 1994;130:191–7.

Cell Death and Differentiation (2005), 1–19

www.nature.com/cdd

Selective induction of ΔFosB in the brain after transient forebrain ischemia accompanied by an increased expression of galectin-1, and the implication of ΔFosB and galectin-1 in neuroprotection and neurogenesis

H Kurushima[1,2], M Ohno[1], T Miura[1], TY Nakamura[3], H Horie[4], T Kadoya[5], H Ooboshi[2], T Kitazono[2], S Ibayashi[2], M Iida[2] and Y Nakabeppu*,[1]

[1] Division of Neurofunctional Genomics, Department of Immunobiology and Neuroscience, Medical Institute of Bioregulation, Kyushu University, Fukuoka 812-8582, Japan
[2] Department of Medicine and Clinical Science, Graduate School of Medical Sciences, Kyushu University, Fukuoka 812-8582, Japan
[3] Department of Molecular Physiology, National Cardiovascular Center Research Institute, Suita, Osaka 565-8565, Japan
[4] Advanced Research Center for Biological Science, Waseda University, 2-7-5 Higashifushimi, Nishitokyo City, Tokyo 202-0021, Japan
[5] CMC R&D Laboratories, Pharmaceutical Division, Kirin Brewery Co., Ltd., Hagiwara 100-1, Takasaki, Gunma 370-0013, Japan
* Corresponding author: Y Nakabeppu, Division of Neurofunctional Genomics, Department of Immunobiology and Neuroscience, Medical Institute of Bioregulation, Kyushu University, Maidashi Higashi-ku, Fukuoka 812-8582, Japan. Tel: +81 92 642 6800; Fax: +81 92 642 6791; E-mail: yusaku@bioreg.kyushu-u.ac.jp

Received 14.12.04; revised 01.3.05; accepted 22.3.05
Edited by H Ichijo

Abstract

Transient forebrain ischemia causes selective induction of ΔFosB, an AP-1 (activator protein-1) subunit, in cells within the ventricle wall or those in the dentate gyrus in the rat brain prior to neurogenesis, followed by induction of nestin, a marker for neuronal precursor cells, or galectin-1, a β-galactoside sugar-binding lectin. The adenovirus-mediated expression of FosB or ΔFosB induced expression of nestin, glial fibrillary acidic protein and galectin-1 in rat embryonic cortical cells. ΔFosB-expressing cells exhibited a significantly higher survival and proliferation after the withdrawal of B27 supplement than the control or FosB-expressing cells. The decline in the ΔFosB expression in the survivors enhanced the MAP2 expression. The expression of ΔFosB in cells within the ventricle wall of the rat brain also resulted in an elevated expression of nestin. We therefore conclude that ΔFosB can promote the proliferation of quiescent neuronal precursor cells, thus enhancing neurogenesis after transient forebrain ischemia.

Cell Death and Differentiation advance online publication, 29 April 2005; doi:10.1038/sj.cdd.4401648

Keywords: AP-1; galectin-1; brain ischemia; neurogenesis; neuronal precursor

Abbreviations: AP-1, activator protein-1; AraC, 1-β-D-arabinofuranosylcytosine; DG, dentate gyrus; EGFP, enhanced green fluorescence protein; GCL, granule cell layer; GFAP, glial fibrillary acidic protein; IRES, internal ribosome entry site; LV, lateral ventricle; PEI, polyethylenimine; SGZ, subgranular zone; SHR, spontaneously hypertensive rat; SVZ, subventricular zone; Tet-Off system, inducible off control system of gene expression by tetracycline; VO, vessel occlusion; WST-8, 2-(2-methoxy-4-nitrophenyl)-3-(4-nitrophenyl)-5-(2, 4-disulfophenyl)-2*H*-tetrazolium

Introduction

In mammals, the regulation of the cell fate to either proliferate, differentiate, arrest cell growth or initiate programmed cell death is the most fundamental mechanism for maintaining normal cell function and tissue homeostasis. Under multiple signaling pathways, Jun and Fos family proteins play important roles as components of the AP-1 (activator protein-1) complex[1,2] to regulate the transcription of various genes involved in cell proliferation, differentiation and programmed cell death.[3,4]

Among the four members of *fos* family genes (*c-fos, fosB, fra-1, fra-2*), only the *fosB* gene forms two mature mRNAs, *fosB* and *ΔfosB*, by alternative splicing,[5] each of which encodes at least three polypeptides by an alternative initiation of translation, called FosB, Δ1FosB, Δ2FosB, and ΔFosB, Δ1ΔFosB, Δ2ΔFosB, respectively.[6,7] The proteins encoded by *ΔfosB* mRNA lack the C-terminal 101-amino-acid region of the proteins encoded by *fosB* mRNA, which contains the motifs responsible for the interaction with TATA-box binding protein (TBP) and TFIID complex and also for the repression of *c-fos* and *fosB* promoters.[5,8] As well as other Fos family proteins, *fosB* gene products form heterodimers with each of the Jun (c-Jun, JunB, JunD) proteins, thereby stimulating the DNA-binding activities. We have previously shown that the proteins encoded by *ΔfosB* mRNA, such as ΔFosB, suppress the Jun transcription-activating ability acting on AP-1-dependent promoters;[5] however, others have demonstrated the ability of ΔFosB to activate the transcription by AP-1.[6,9] The ectopic expression of ΔFosB in transgenic mice revealed that ΔFosB indeed either upregulates or downregulates the expression of subsets of genes in the brain.[10,11] It is thus likely that the *fosB* gene products, especially ΔFosB, play an important role in the modulation of the gene expression regulated by AP-1.

In most types of rodent tissue, the *fosB* expression is either absent or barely detectable, while a basal expression of *fosB* is detected in some neurons scattered throughout the cerebral cortex and the hippocampus.[12] We have shown that the expression of the *fosB* gene, as well as *c-fos* or *c-jun*, is highly induced in the dentate gyrus (DG) of the hippocampus prior to the delayed neuronal loss in the CA1 subfield after transient

forebrain ischemia.[13] It has also been well established that neurogenesis can be induced in the adult mammalian brain after several forms of brain damage, such as seizure and transient ischemia, and it is restricted to specific regions such as the subventricular zone (SVZ) and DG of the hippocampus.[14–17] We previously found that ΔFosB, and to a lesser extent FosB, triggers one round of proliferation in the quiescent rat embryo cell lines rat 3Y1 and rat 1a followed by a different cell fate such as morphological alteration or delayed cell death, respectively.[18–22] We have also shown that the expression of galectin-1, one of the major β-galactoside sugar-binding lectins, is induced by ΔFosB in those cells, and it is required for the proliferative activation of quiescent rat 1a cells by ΔFosB,[21] thus indicating that galectin-1 is one of the functional targets of ΔFosB to modulate the cell fate, thus suggesting that ΔFosB, together with galectin-1, may play a critical role in determining the cell fate observed in the damaged brain.

In the present study, we found the expression of ΔFosB but not FosB to be selectively induced in cells within the ventricle wall, which also highly expressed nestin, a marker for neuronal precursor cells, as well as in the DG and CA1 subfield after transient forebrain ischemia in the rat brain. In a rat embryonic cortical cell culture, adenovirus-mediated expression of ΔFosB, and to a lesser extent FosB, promoted survival of nestin- and/or glial fibrillary acidic protein (GFAP)-positive cells after withdrawal of B27 trophic support, and also tended to induce their selective proliferation. The expression of ΔFosB in cells within the ventricle wall of the rat brain also resulted in an elevated expression of nestin. Furthermore, we demonstrated that the expression of galectin-1 is induced by FosB or ΔFosB in the embryonic cortical cells as well as in the hippocampus after transient forebrain ischemia.

Results

Expression of ΔFosB in brain after transient forebrain ischemia accompanied by the insult-induced neurogenesis

We previously reported the FosB and ΔFosB expression in hippocampus to be persistently elevated 2–48 h after transient forebrain ischemia produced by the four-vessel occlusion (4-VO) method, prior to the delayed CA1 neuronal loss in male Wister rats.[13] In the present study, we applied the 2-VO method to spontaneously hypertensive rats (SHR) in order to induce transient forebrain ischemia with a simple operation.[23] The CA1 neuronal loss was apparent 2–7 days after ischemic insult (Figure 1a and f). We then examined the FosB and ΔFosB expression in this model using two different antibodies against the *fosB* gene products. In the control rats, a weak immunoreactivity to the FosB(102) antibody, which recognizes both FosB and ΔFosB, was detected in some neurons scattered throughout the brain cortex and in the hippocampus (Figure 1b–e). At 2 days after the ischemic insult, there was a marked increase in the number of neurons that displayed a strong FosB(102) immunoreactivity in the entire region of the hippocampus (Figure 1g–j). Especially in the DG, the extent of immunoreactivity significantly varied from neuron to neuron in the granule cell layer (GCL) (Figure 1h). Cells with smaller nuclei exhibited a stronger immunoreactivity and such cells were more abundant in the subgranular zone (SGZ) of the DG and CA1 subfield. A strong FosB(102) immunoreactivity was also detected in the ependymal or subependymal cells within the lateral ventricle (LV) wall only after ischemic insult (Figure 1j). The brain sections shown in Figure 1 were subjected to double immunohistochemistry with anti-nestin sequentially. A moderate nestin immunoreactivity was detected throughout the cerebral cortex and in the hippocampus only after ischemic insult (Figure 1g–j). Some cells in SGZ with a strong FosB(102) immunoreactivity also exhibited a strong nestin immunoreactivity (Figure 1h), and such double-positive cells were also detected in the CA1 subfield (Figure 1i). Most of the ependymal or subependymal cells within the LV wall with FosB(102) immunoreactivity exhibited a strong nestin immunoreactivity (Figure 1j). Such increased immunoreactivities of FosB(102) and nestin were also apparent in cells within the third ventricle wall after ischemia (data not shown).

FosB(C) antibody against the C-terminal domain of FosB, which is missing in ΔFosB,[5] also exhibited an increased immunoreactivity in the hippocampus after the ischemic insult (Figure 2b and d). However, the FosB(C) immunoreactivity was detected in less than half of the hippocampal neurons, while FosB(102) immunoreactivity was detected in almost all neurons in the hippocampus (Figure 2a and c). There was no FosB(C) immunoreactivity detected in the ependymal or subependymal cells within the LV wall; however, most of them exhibited a strong nuclear FosB(102) immunoreactivity (Figure 2c and d). Most of the cells within the LV wall exhibited a strong nestin immunoreactivity in their cytoplasm after ischemic insult (Figure 2e).

As a result, we concluded that more than half of hippocampal neurons predominantly express ΔFosB, while the others express both FosB and ΔFosB. Furthermore, the ependymal or subependymal cells within the LV wall express high levels of nestin and ΔFosB but not FosB after the ischemic insult. It was noteworthy that the FosB(102) immunoreactivity in the brain apparently returned to the basal level 7 days after the insult (data not shown).

Proliferative response in the brain after transient forebrain ischemia

In adult rodent brains, it has been established that DG in hippocampal formation and the SVZ are two major sites of high-density cell division,[15] and that such cell division is induced by various types of brain stress such as the ischemic insult.[14,16] To confirm whether such cell division occurs in the brain of SHR after the ischemic insult, bromodeoxyuridine (BrdU) was administered to the rats once a day for a week either with or without the insult. There was a significant increase in the number of BrdU-labeled cells in the hippocampus 7 days after the ischemic insult in comparison with the control brain (Figure 3a and f). BrdU-labeled cells were more abundant in the CA1 subfield and DG than in the CA3 subfield (Figure 3g–i). In this experiment, we observed a few foci of BrdU-positive cells in the cerebral cortex (Figure 3j), thus suggesting that the cerebral cortex of SHR exhibits hypervulnerability or enhanced proliferative response to the ischemic

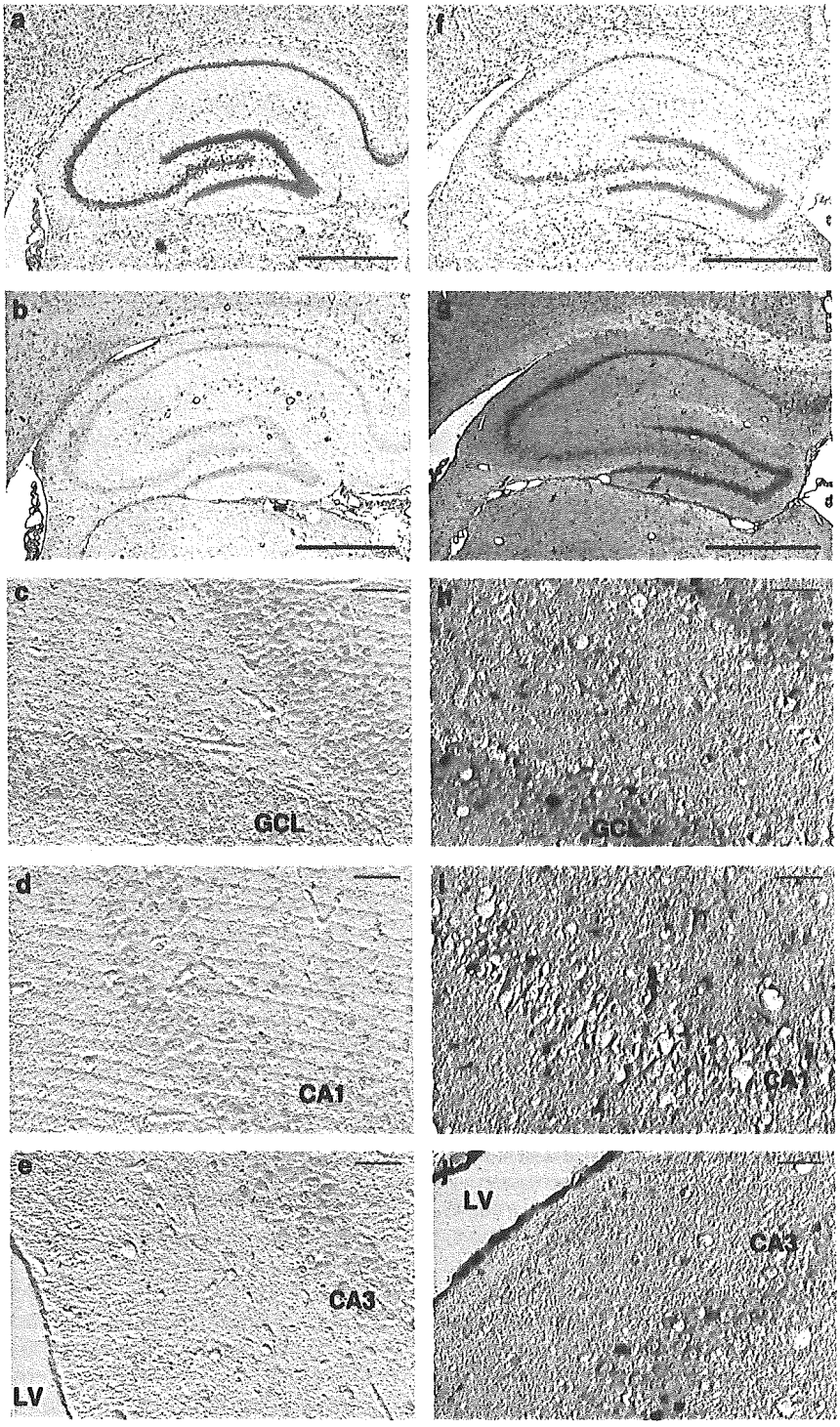

Figure 1 Expression of *fosB* gene products in nestin-positive cells after transient forebrain ischemia. In the control animals (**a–e**), a weak FosB(102) immunoreactivity (**b–e**, brown) was detected in the neurons scattered within the cerebral cortex and hippocampus, and nestin immunoreactivity (**b–e**, blue) was barely detectable throughout the brain. At 2 days after 20 min of forebrain ischemia (**f–j**), neuronal loss in the CA1 subfield of the hippocampus was assessed by Cresyl violet staining (**a, f**). FosB(102) immunoreactivity was dramatically elevated in neurons within the cerebral cortex and hippocampus (**g–j**, brown), and nestin immunoreactivity was also moderately elevated throughout the brain (**g–j**, blue). In the DG (**c, h**), FosB(102) immunoreactivity was detected in most of the granule cells, but a few were positive for nestin immunoreactivity in the lesioned rat. In the CA1 subfield (**d,i**), double-positive cells with FosB(102) and nestin immunoreactivity were detected only in the lesioned rat. In the CA3 subfield (**e, j**), most of the pyramidal cells in the lesioned rats were positive for FosB(102) immunoreacitivity, but a few were positive for nestin immunoreactivity. In the ependymal cells within the LV wall (**e, j**), strong immunoreactivities both for FosB(102) and nestin were simultaneously detected only in the lesioned rat. Scale bars: 1 mm (**a, b, f, g**), 50 μm (**c–e, h–j**)

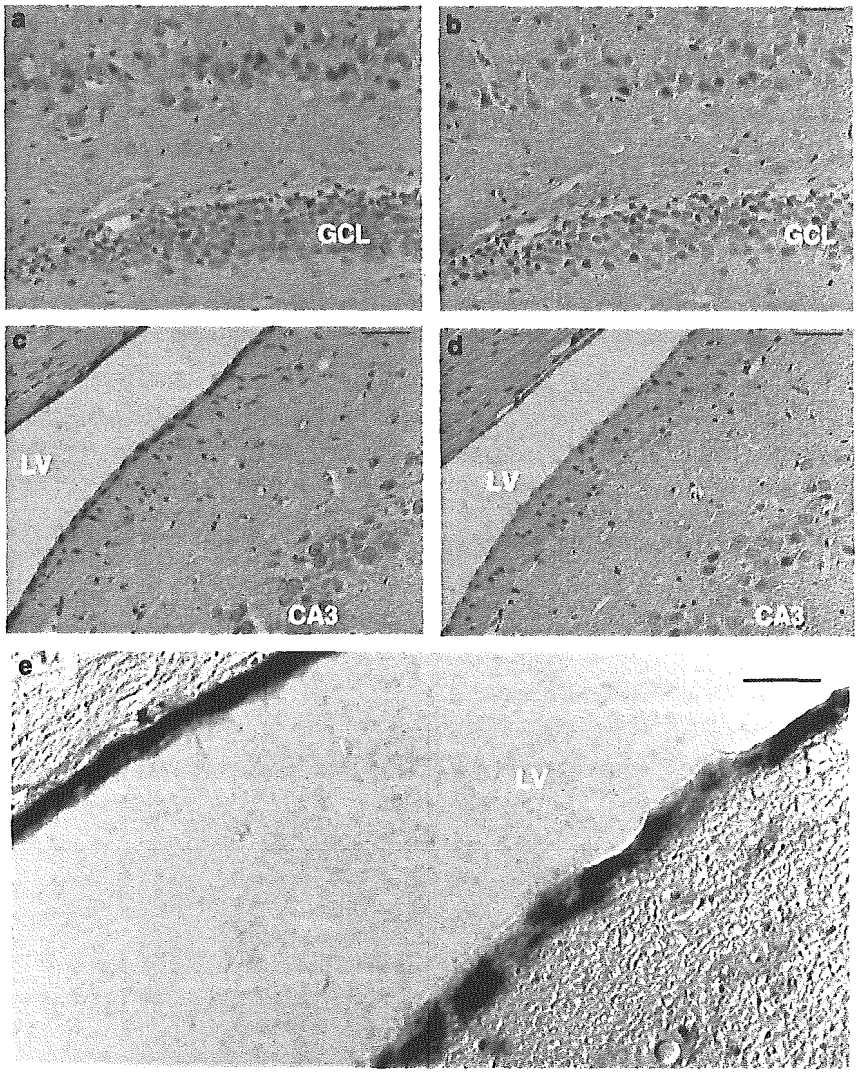

Figure 2 ΔFosB is selectively expressed in the ependymal cells within the LV wall after transient forebrain ischemia. At 2 days after forebrain ischemia, FosB(102) immunoreactivity (**a**, **c**, **e**, brown) was detected in most of the dentate granule cells, CA3 pyramidal cells and ependymal cells within the LV wall. However, FosB(C) immunoreactivity was detected in some of the dentate granule cells or CA3 pyramidal cells but none of the ependymal cells within the LV (**b**, **d**). Most of the ependymal cells in the LV wall in the lesioned rat exhibited the nestin immunoreactivity in their cytoplasm (**e**, blue for nestin). As shown in Figure 11, both antibodies had the same immunoreactivity toward FosB, but anti-FosB(C) never reacted with ΔFosB. Scale bars: 50 μm (**a–d**), 20 μm (**e**)

insult. Proliferative responses in the brain are known to be accompanied by an increased expression of GFAP and nestin. We therefore examined the expression of nestin and GFAP in the brain with or without the ischemic insult (Figure 3k–v). In the ischemic brain, the number of nestin-expressing cells increased dramatically 7 days later, and their distribution was almost identical to that of BrdU-labeled cells in the hippocampus (Figure 3f–h, l, n and o). However, in the cerebral cortex, foci of BrdU-labeled cells were surrounded by nestin-positive cells (Figure 3f, j, l and p). Expression of GFAP in the lesioned rat was more significantly elevated surrounding the foci of BrdU-labeled cells in the cerebral cortex, as well as in the entire region of hippocampus, in comparison with that of nestin (Figure 3q–v).

As a result, we confirmed the expression of ΔFosB, and to a lesser extent FosB, to be persistently elevated in a subset of cells at the two sites of high-density cell division in the brain after the ischemic insult, thus suggesting that ΔFosB may play a role in the regulation of such cell division in response to brain insult.

Adenovirus-mediated expression of *fosB* gene products in a rat embryonic cortical cell primary culture

The selective expression of ΔFosB in cells within the ventricle walls after ischemic insults strongly suggests that ΔFosB plays an important role during the stress response in the brain. Since *fosB* gene products possess the potential to initiate proliferation of quiescent cells,[18–22] we hypothesize that ΔFosB induces the proliferative activation of neuronal stem cells or precursor cells in the ischemic brain.

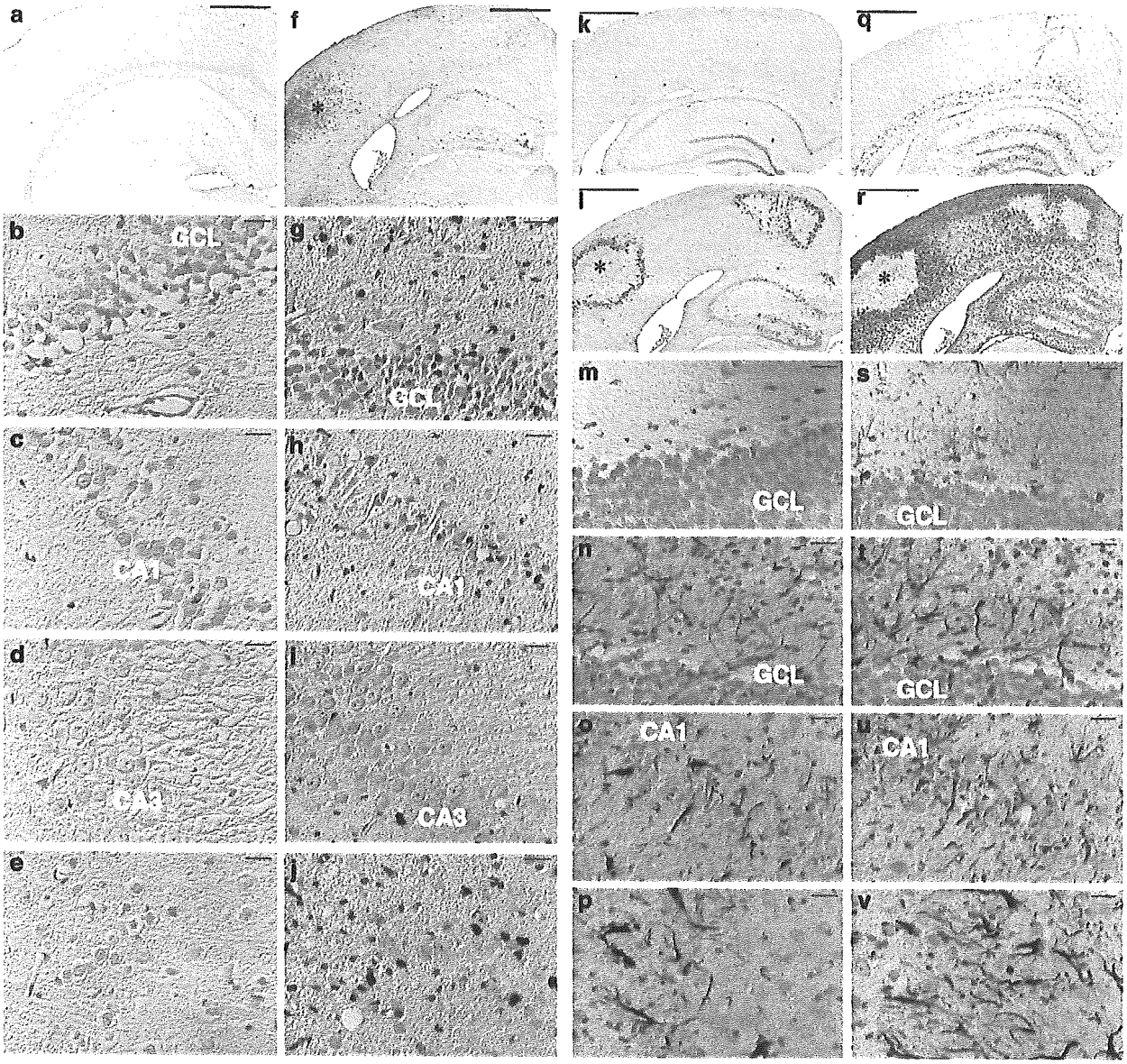

Figure 3 Proliferative responses in brain after transient forebrain ischemia. BrdU (50 mg/kg) was administered intraperitoneally to the control rats (**a–e, k, m, q, s**) and to the rats with transient forebrain ischemia (**f-j, l, n-p, r, t–v**) once a day for a week. (**a–j**) Anti-BrdU immunostaining; (**k–p**) anti-nestin immunostaining; (**q–v**) anti-GFAP immunostaining. In the control animals (**a, k**), BrdU-labeled or nestin-positive cells were barely detectable throughout the brain. However, a weak GFAP immunoreactivity was detected in the hippocampus of the control animals (**q**). In the lesioned rats (**f, l, r**), the brain regions containing BrdU-labeled cells shown with asterisks were surrounded by nestin-positive and GFAP-positive cells. In the lesioned rats, a substantial number of cells in the DG (**g, n, t**), CA1 subfield (**h, o, u**) and subregions in the cerebral cortex (**j, p, v**), but not the CA3 subfield (**i**) exhibited strong BrdU, nestin and GFAP immunoreactivities. Scale bars: 1 mm (**a, f, k, l, q, r**), 20 μm (**b–e, g–j, m–p, s–v**)

To evaluate this hypothesis, we constructed adenovirus vector expressing *fosB* gene products under the control of the Tet-Off system (inducible off control system of gene expression by tetracycline). In order to visualize the adenovirus-infected cells, enhanced green fluorescence protein (EGFP) was coexpressed using an internal ribosome entry site (IRES) bicistronic expression system, which was placed downstream of FosB or ΔFosB cDNA. The expression of each *fosB* gene product was confirmed by Western blotting of rat 1a cells infected with each adenovirus together with Adeno-X Tet-Off virus expressing a tetracycline-controlled transactivator, tTA. Adenovirus carrying FosB cDNA produced 45, 35 and 30-kDa polypeptides, which most likely correspond to the polypeptides translated from the first, second and third methionine codons of FosB mRNA, while adenovirus carrying ΔFosB cDNA produced 35, 25 and 22-kDa polypeptides, corresponding to the translation products by the alternative translation initiation,[7] reacted with anti-FosB(102) (Figure 4a). Confocal laser-scanning fluorescence microscopy with the same antibody revealed that FosB or ΔFosB was expressed only in cells

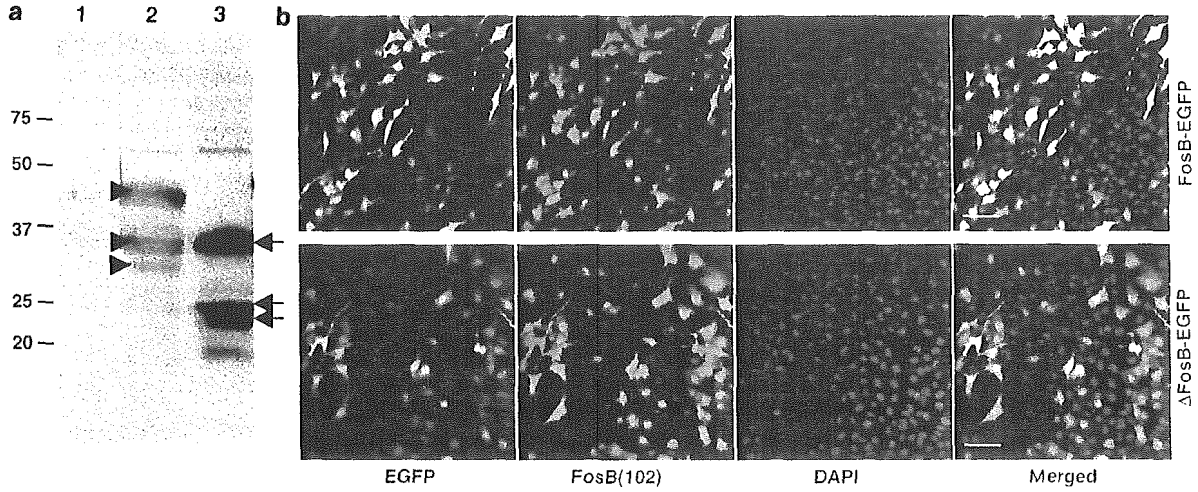

Figure 4 Expression of FosB and ΔFosB by recombinant adenovirus. (**a**) Western blotting analysis. Cell lysates prepared from rat 1a cells infected with recombinant adenovirus encoding EGFP alone (lane 1), FosB-EGFP (lane 2) and ΔFosB-EGFP (lane 3), together with Adeno-X Tet-Off virus, were subjected to a Western blot analysis using FosB(102) antibody. The arrowheads indicate the alternative translation initiation products from *fosB* mRNA, and the arrows indicate those from *ΔfosB* mRNA. (**b**) Laser-scanning fluorescence microscopy with anti-FosB(102). Rat 1a cells infected with each recombinant adenovirus (FosB-EGFP, ΔFosB-EGFP), as indicated on the right side, were fixed, and the nuclei were counterstained with DAPI. Confocal images were obtained by laser-scanning fluorescence microscopy after reaction with anti-FosB(102). Each fluorescence is shown in green (EGFP fluorescence), red (FosB(102) immunofluorescence) and blue (DAPI). Merged: the merged view of the three fluorescences. Scale bars, 100 μm

infected with the recombinant adenoviruses encoding FosB or ΔFosB, and both were localized in the cytoplasm as well as in the nuclei (Figure 4b). The expression of FosB or ΔFosB from the adenoviral vector was completely abolished in the presence of a minimum of 5 ng/ml doxycycline (data not shown).

We next applied the adenoviruses to rat embryonic cortical cells to induce the expression of FosB and ΔFosB in neuronal precursor cells. We prepared embryonic cortical cells from the brain cortex together with the hippocampus of 18-day-old rat embryos; thus the embryonic cortical cells used in this study contain the neuronal precursor cells derived from the SVZ and hippocampus. Adenovirus-mediated expression of *fosB or ΔfosB* mRNA in rat embryonic cortical cells was confirmed by semiquantitative RT-PCR analyses (Figure 5a and b), thus indicating that each recombinant adenovirus produces only the *fosB* or *ΔfosB* transcript, respectively, and that their levels were almost equivalent.

Since it has been shown that neuronal precursor cells, such as radial glias or radial cells, which occupy the cortical and ventricular surfaces, express the highest level of an adenovirus receptor, CAR, adenovirus was proved to have a high *probability of infecting those cells.*[24,25] Therefore, rat embryonic cortical cells were infected with each recombinant adenovirus at MOI = 1, and EGFP-positive cells, which represented adenovirus-infected cells, were mostly MAP2 or β-tubulin III-negative (data not shown), thus indicating that few mature neurons were infected with recombinant adenoviruses. The morphology of cells expressing EGFP was likely to be different from each other (Figure 5c–e). More than half of all EGFP-positive cells without FosB or ΔFosB expression exhibited a typical morphology of astrocytes, namely the *irregular and roughly star-shaped cell bodies. However,* EGFP-positive cells expressing FosB or ΔFosB tended to exhibit a unipolar or bipolar shape.

In a rat embryonic cortical cell primary culture, immunohistochemistry with three Jun-specific antibodies revealed the expression of FosB and ΔFosB to be accompanied by increased expression of c-Jun, JunB and JunD (Figure 5c–e). FosB and ΔFosB were largely detected in the cytoplasm; however, an increased JunD immunoreactivity was apparently detected in the nuclei of cells expressing FosB or ΔFosB among the three Jun proteins. Semiquantitative RT-PCR analyses showed the *JunB* mRNA levels, to a lesser extent

Figure 5 Adenovirus-mediated expression of FosB and ΔFosB in embryonic cortical cells and the coexpression of Jun proteins. (**a**) Schematic representation of *fosB* and *ΔfosB* mRNAs. The closed regions indicate the common sequences for the two mRNAs while the open region indicates the 140-base sequence that is alternatively spliced out in *ΔfosB* mRNA. The primers used to amplify the common region (*fosB-5'*) for *fosB* and *ΔfosB* mRNA are shown by arrows and those used to amplify the sequence (*fosB-3'*) within the 140-base sequence are shown by arrowheads. Specific TaqMan probes for the *fosB-5'* and *fosB-3'* sequences are shown by a gray and hatched box, respectively. (**b**) Expression of *fosB* and *ΔfosB* mRNAs in rat embryonic cortical cells after the infection of adenovirus encoding EGFP alone, FosB-EGFP and ΔFosB-EGFP. Rat embryonic cortical cells infected with each recombinant adenovirus (EGFP, FosB-EGFP, ΔFosB-EGFP), as indicated on the bottom, were cultured for 2 days after the withdrawal of B27 trophic support. The relative amount of each RT-PCR product for *Gapdh* product was determined by monitoring the PCR product in real time. Gray bar: PCR products from the common region (*fosB-5'*); hatched bar: PCR products from the primers specific for *fosB* mRNA (*fosB-3'*). (**c–e**) The coexpression of Jun proteins in rat embryonic cortical cells induced by FosB or ΔFosB. Rat embryonic cortical cells infected with each recombinant adenovirus (EGFP alone, FosB-EGFP, ΔFosB-EGFP), as indicated on the left side, were cultured for 3 days, and then were fixed and subjected to immunofluorescent microscopy with FosB(102) and each Jun-specific antibody (**c**: c-Jun; **d**: JunB; **e**: JunD). Each fluorescence is shown in green (EGFP fluorescence), red (FosB(102) immunofluorescence) and blue (Jun immunofluorescence). Merged: the merged view of the three fluorescences. Scale bars, 50 μm

c-jun, to increase more than 2.5-fold in FosB-expressing embryonic cortical cells, but no such increase was seen in ΔFosB-expressing embryonic cortical cells, in comparison to the cells expressing only EGFP (Table 1). On the other hand, *JunD* mRNA levels in embryonic cortical cells expressing FosB and ΔFosB decreased to 83 and 73% of the levels in EGFP-expressing cells, respectively. The mRNA levels of *Cdk5* and *GluR2* whose expressions were reported to be induced in the striatal neurons by ΔFosB,[10,11] did not increase at all, or rather slightly decreased, especially in embryonic

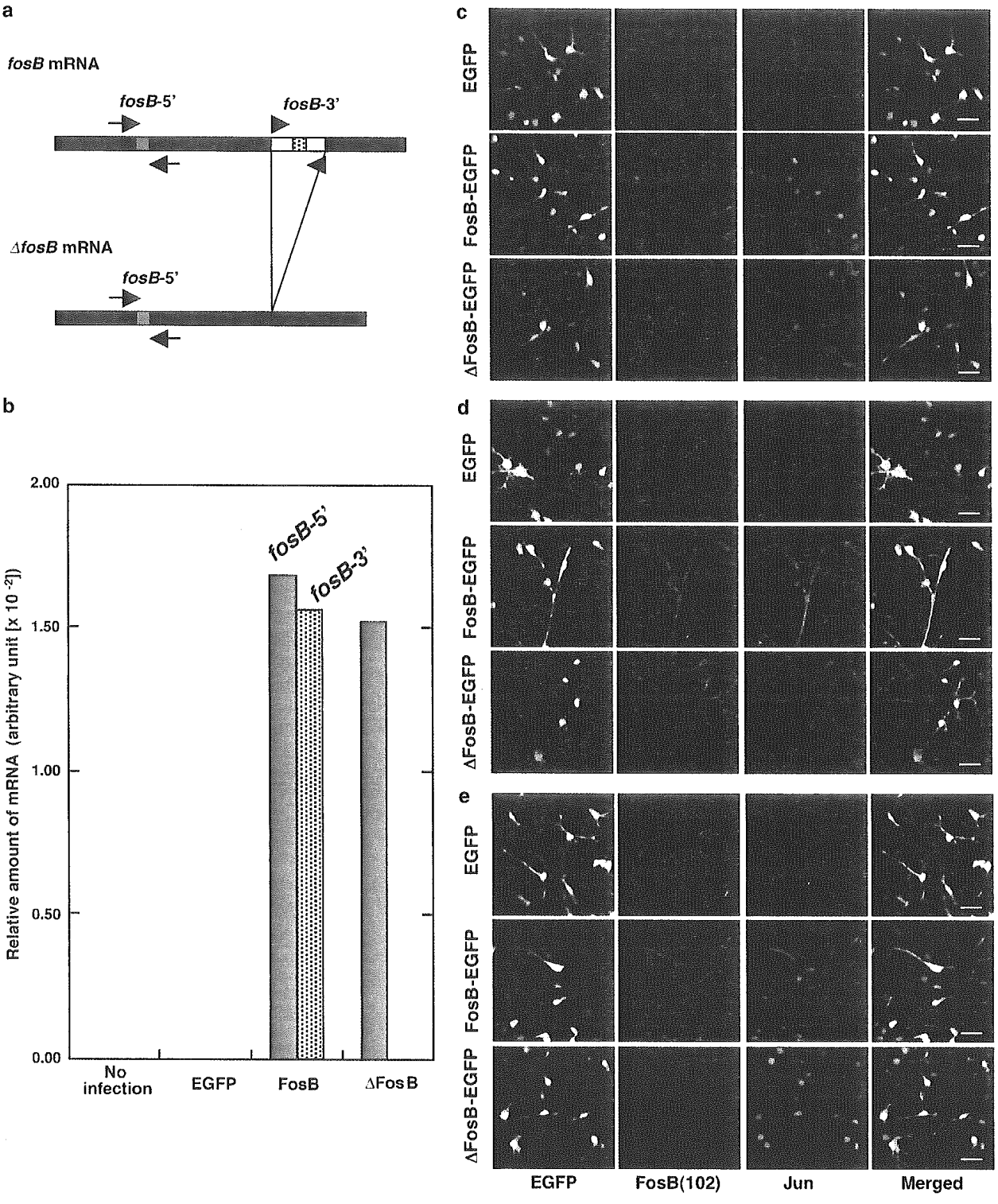

Table 1 *Altered gene expression in embryonic cortical cells expressing FosB or ΔFosB*

	Relative level of transcript in cortical cells expressing[a]		
Gene	**EGFP**	**FosB**	**ΔFosB**
c-*Jun*	1.00±0.10	1.17±0.05	1.00±0.18
JunB	1.00±0.09	2.65±0.22	1.14±0.04
JunD	1.00±0.04	0.83±0.01	0.73±0.02
Mmp3	ND	ND	ND
Cdk5	1.00±0.07	1.00±0.09	0.94±0.02
GluR2	1.00±0.10	0.95±0.04	0.90±0.05
Gfap	1.00±0.05	1.68±0.11	1.43±0.01
Nestin	1.00±0.07	1.56±0.10	1.66±0.27

Rat embryonic cortical cells were infected with each recombinant adenovirus encoding EGFP alone, FosB-EGFP or ΔFosB-EGFP, and then were cultured for 4 days in the presence of B27 supplement. At 2 days after the culture medium was changed to a Neurobasal medium lacking B27 supplement, total RNA were prepared and subjected to RT-PCR and amplification was monitored in real time. Experimental values obtained for each transcript were divided by the values for *Gapdh* mRNA in the same preparation. Level of each transcript was normalized to that in cells expressing EGFP alone. [a]Mean values with S.D. from three independent PCR are shown. ND: not detected

cortical cells expressing ΔFosB. Regardless of either FosB or ΔFosB expression, no detectable *Mmp3* mRNA was observed, whose expression is known to be upregulated by FosB but not ΔFosB in rat 1a cells as one of the AP-1-responsive genes.[18]

ΔFosB stimulates the proliferation of the embryonic cortical cells after the withdrawal of B27 trophic support

To examine the biological significance of FosB or ΔFosB expression in the embryonic cortical cells, viability of adenovirus-infected cells was determined after the withdrawal of the B27 trophic support, which is essential for their maintenance from the cultured medium.[26,27] As shown in Figure 6a, the culture that received adenovirus expressing EGFP alone exhibited a slight increase of cells within the first 2 days after B27 withdrawal and thereafter a decreased cell viability was observed, as determined by 2-(2-methoxy-4-nitrophenyl)-3-(4-nitrophenyl)-5-(2,4-disulfophenyl)-2*H*-tetrazolium (WST-8) formazan assay. In contrast, the cultures that received adenovirus expressing FosB or ΔFosB exhibited more growth than the control cells within the first 2 days, and showed a decreased viability on the 4th day. At 1 week after B27 withdrawal, only ΔFosB-expressing cells recovered significantly and increased their viability.

In order to identify cells that survived after B27 withdrawal, the cells were examined under fluorescent microscopy and the number of EGFP-positive cells was determined. As shown in Figure 6b, the number of EGFP-positive cells in culture infected with adenovirus expressing EGFP alone decreased continuously after B27 withdrawal and only 30% of the EGFP-positive cells survived on the 8th day after B27 withdrawal. The expression of FosB maintained the number of EGFP-positive cells for the first 4 days; however, the number

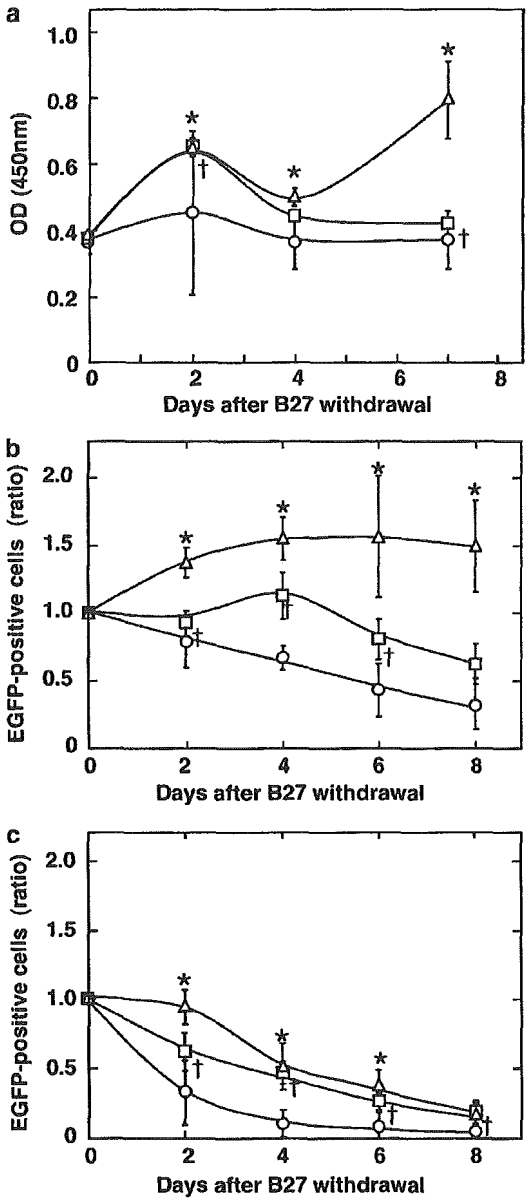

Figure 6 ΔFosB, and to a lesser extent FosB, induced proliferation of rat embryonic cortical cells in the absence of B27 supplement. (**a**) Cell viability. Rat embryonic cortical cells were infected with each recombinant adenovirus, and then were cultured for 3 days in the presence of B27 supplement. After the culture medium was changed to Neurobasal medium lacking B27 supplement, cell viability was determined using WST-8 assay as described in Materials and Methods, every other day. (**b**) Proliferation of EGFP-positive cells. After the culture medium was changed to a Neurobasal medium lacking B27 supplement, the number of EGFP-positive cells in the same field was counted every other day. (**c**) Survival of EGFP-positive cells. After the infection of each recombinant adenovirus, the rat embryonic cortical cells were cultured for 3 days in the presence of 10 μM AraC and B27 supplement. After the culture medium was changed to a Neurobasal medium lacking B27 supplement, the number of EGFP-positive cells in the same field was counted every other day. Circle: EGFP alone; squares: FosB-EGFP; triangles: ΔFosB-EGFP. The data are shown with the means ± S.D. (four independent experiments). The cell number was normalized to that of day 0. Statistical significance ($P<0.05$) is indicated by † for FosB-EGFP and * for ΔFosB-EGFP, in comparison with EGFP alone

decreased thereafter and about 60% of EGFP-positive cells survived on the 8th day. In contrast, embryonic cortical cells infected with adenovirus expressing ΔFosB increased the number of EGFP-positive cells more than 1.5 times within 4 days after B27 withdrawal, and most EGFP-positive cells survived thereafter.

We next examined the effect of the cytidine analog, 1-β-D-arabinofuranosylcytosine (AraC) on the embryonic cortical cells. AraC inhibits DNA replication, and thus only postmitotic cells, such as neurons, can survive. Most of the EGFP-positive cells in culture that received adenovirus expressing EGFP alone disappeared within the first 4 days after B27 withdrawal, while the expression of ΔFosB, and to a lesser extent FosB, significantly improved the survival of EGFP-positive cells (Figure 6c).

It is likely that ΔFosB, and to a lesser extent FosB, stimulates embryonic cortical cell proliferation even in the absence of B27 trophic support. We next examined whether ΔFosB or FosB stimulates DNA synthesis in embryonic cortical cells. In the presence of BrdU, embryonic cortical cells were infected with each adenovirus, and were cultured for 3 days. The incorporation of BrdU into nuclear genomes was monitored by immunofluorescence microscopy (Figure 7 and Table 2). In the culture receiving adenovirus expressing EGFP alone, none of the EGFP-positive cells incorporated BrdU. On the other hand, about 6% of the EGFP-positive cells in culture receiving adenovirus expressing FosB or ΔFosB were strongly labeled with anti-BrdU antibody. We thus concluded that FosB and ΔFosB stimulate the cell proliferation of embryonic cortical cells, and that ΔFosB, and to a lesser extent FosB, promotes cell survival after B27 withdrawal.

Because there were quite a few BrdU-labeled and EGFP-negative cells around EGFP-positive cells, some factor(s) secreted from cells expressing FosB or ΔFosB may promote their proliferation (Figure 7).

Coexpression of galectin-1 and nestin in the embryonic cortical cells expressing FosB or ΔFosB, as well as in the brain after transient ischemia

In rat 1a cells, the ectopic expression of ΔFosB increased the expression of galectin-1, which was partly responsible for their proliferation induced by ΔFosB.[20,21] We examined the expression of galectin-1 in the cortical cells after FosB or ΔFosB expression, since galectin-1 is known to be a secretory

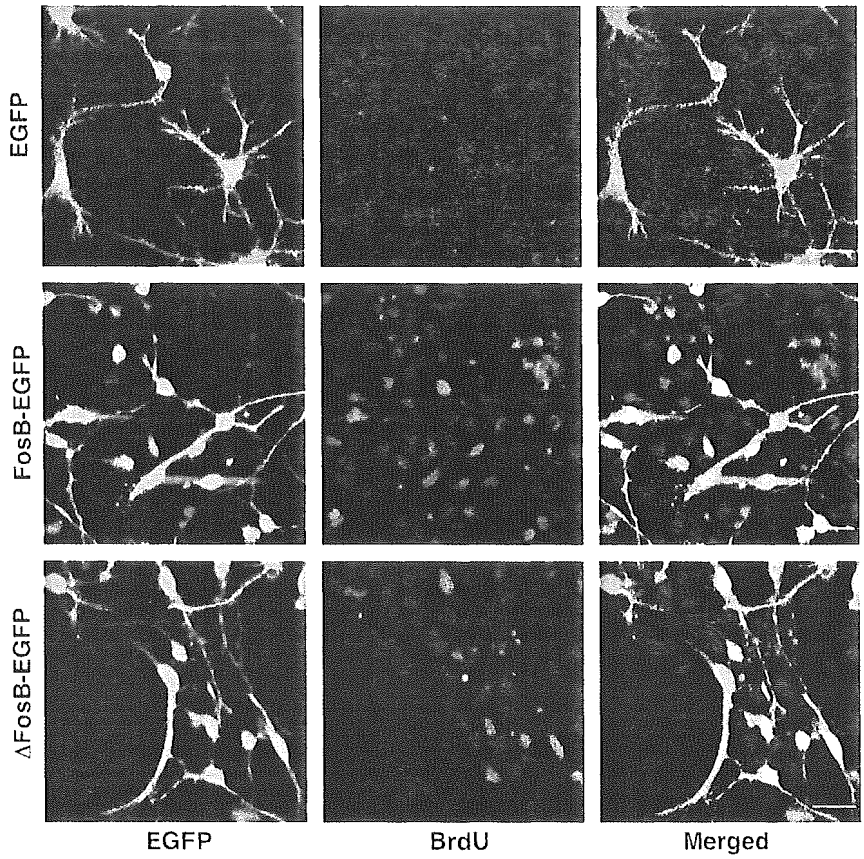

Figure 7 DNA synthesis in adenovirus-infected rat embryonic cortical cells. Rat embryonic cortical cells were infected with each recombinant adenovirus encoding EGFP alone, FosB-EGFP and ΔFosB-EGFP, as indicated on the left side, and were cultured in the presence of B27 supplement and 10 μM BrdU for 3 days. The cells were fixed and subjected to immunofluorescence microscopy with anti-BrdU antibody. Green: EGFP fluorescence; red: anti-BrdU immunofluorescence; merged: the merged view of the two fluorescences. Scale bars, 50 μm

Table 2 DNA synthesis in adenovirus-infected rat embryonic cortical cells

Adenovirus	No. of EGFP$^+$ cells	No. of BrdU$^+$ cells	% BrdU$^+$ cells
EGFP	116	0	0
FosB-EGFP	177	11	6.2
ΔFosB-EGFP	180	10	5.6

Rat embryonic cortical cells were infected with recombinant adenoviruses and then were cultured in the presence of B27 supplement and 10 μM BrdU for 3 days. The cells were fixed and subjected to immunofluorescence microscopy with anti-BrdU antibody as shown in Figure 7. The number of cells in areas of the same size was counted. Among EGFP-positive cells, only cells exhibiting a strong BrdU immunoreactivity were counted as BrdU$^+$

factor that can regulate cell fate such as proliferation or apoptosis.[22] As shown in Figure 8a, galectin-1 was barely detected in the embryonic cortical cells expressing EGFP alone; however, a significantly higher level of galectin-1 as well as nestin was detected in the embryonic cortical cells expressing FosB or ΔFosB. We next examined the effects of galectin-1 on proliferation of the embryonic cortical cells. In the presence of a low dose of recombinant galectin-1α (50 pg/ml), the proliferation of the embryonic cortical cells was slightly, but significantly, promoted in comparison to that in the absence of galectin-1α (Figure 8b), thus indicating that galectin-1α, as one type of secretory factor, has a potential to promote the proliferation of embryonic cortical cells. Interestingly, a higher dose of galectin-1α (5 μg/ml) or galectin-1β (50 pg/ml or 5 μg/ml, data not shown), which is known to be a variant form of galectin-1,[22] exhibited a much weaker effect.

We next examined the expression of galectin-1 in the rat brain after transient forebrain ischemia by confocal laser-scanning fluorescence microscopy (Figure 8c). In the control brain, the expression of neither galectin-1 nor nestin was detectable, while a significantly higher level of galectin-1 was detected in the hippocampus after ischemia, where the nestin expression also showed a dramatic increase. Most of the nestin-positive cells in the hippocampus expressed galectin-1, while the nestin-positive cells within the ventricle wall did not express galectin-1 (data not shown).

Expression of neuronal markers in the rat embryonic cortical cells expressing FosB or ΔFosB

In order to identify the cell type whose proliferation was stimulated by FosB or ΔFosB, we examined the expression of various neuronal markers such as MAP2, β-tubulin III, nestin and GFAP in the rat embryonic cortical cells maintained in the absence of B27 supplement. The majority of the embryonic cortical cells were MAP2- or β-tubulin III-positive matured neurons; however, they were exclusively EGFP-negative (data not shown). In contrast, EGFP-positive cells were largely nestin-positive, and some of them were also GFAP-positive, regardless of the FosB or ΔFosB expression (Figure 9 and Table 3). EGFP-positive cells in the culture that received adenovirus expressing EGFP alone exhibited the typical morphology of astrocytes with GFAP expression, namely the irregular and roughly star-shaped cell bodies with weaker immunoreactivity to anti-nestin. A quarter of nestin-positive cells were GFAP-negative and they were somehow morphologically different from the rest (Figure 9). In contrast, EGFP-positive cells expressing FosB exhibited mostly a bipolar shape with a stronger immunoreactivity to anti-nestin, and less than a quarter of them exhibited immunoreactivity to anti-GFAP. We found more abundant EGFP-positive cells in the culture receiving adenovirus expressing ΔFosB in comparison to those expressing FosB, and most of them also exhibited a strong immunoreactivity to anti-nestin (Table 3). ΔFosB-expressing cells exhibiting immunoreactivity both to anti-nestin and anti-GFAP possessed dendrite-like structures with elongated neurite-like structures, while those with a single immunoreactivity to anti-nestin exhibited a bipolar shape. As shown in Table 1, the mRNA levels of *Gfap* and *Nestin* increased from 43 to 68% in embryonic cortical cells expressing either FosB or ΔFosB, in comparison to cells expressing only EGFP.

ΔFosB can maintain the immature property of neuronal precursor cells and the decline of ΔFosB may play an important role in neuronal maturation

Rat embryonic cortical cells expressing FosB or ΔFosB in the absence of B27 supplement, as shown in Figure 9, most likely proliferate neuronal precursor cells. To address this question, we turned either the FosB or ΔFosB expression off by adding doxycycline to the culture. We then monitored the expression of MAP2 in the EGFP-positive cells in the presence of B27 supplement. As shown in Figure 10, 4 days after the addition of doxycycline, MAP2-positive cells appeared only in the culture receiving adenovirus expressing ΔFosB but not FosB or EGFP alone (data not shown). Unfortunately, doxycycline also decreased the expression of EGFP; therefore, we could observe only a small number of EGFP-positive cells in the experiment. In the absence of doxycycline, EGFP-positive cells were more abundant but none of the EGFP-positive cells exhibited immunoreactivity to anti-MAP2 (Figure 10).

Figure 8 The coexpression of galectin-1 and nestin in the embryonic cortical cells expressing FosB or ΔFosB as well as in the brain after transient forebrain ischemia. (**a**) Rat embryonic cortical cells were infected with each recombinant adenovirus encoding EGFP alone, FosB-EGFP and ΔFosB-EGFP, as indicated on the left side, and then were cultured for 4 days in the presence of B27 supplement. At 2 days after the culture medium was changed to a Neurobasal medium lacking B27 supplement, the cells were fixed and subjected to immunofluorescence microscopy. Green: EGFP fluorescence; red: nestin immunofluorescence; blue: GFAP immunofluorescence; merged: the merged view of the three fluorescences. Scale bars, 50 μm. (**b**) Galectin-1α promotes proliferation of the cortical cells *in vitro*. Rat embryonic cortical cells were cultured in the Neurobasal medium with B27 supplement in the absence (control) or presence of galectin-1α (50 pg/ml or 5 μg/ml). At 4 days later, the cell viability was determined using a WST-8 assay. $^*P<0.05$, compared with the control. (**c**) Galectin-1 is expressed in the hippocampus formation after transient forebrain ischemia. The brain sections were prepared from the rats 7 days after the transient forebrain ischemia, and then were subjected to confocal laser-scanning microscopy after a reaction with anti-rhGal-1 (red) or anti-nestin (green) with a proper Alexa-labeled second antibody. Galectin-1 and nestin were mostly colocalized in the hippocampus. Blue: DAPI; Merged: the merged view of the three fluorescences. Scale bars: 25 μm

ΔFosB expression in cells within the ventricle wall induces the expression of nestin but not GFAP

In order to examine whether ΔFosB expression in the ependymal or subependymal cells within the ventricle wall alters their phenotype, recombinant adenovirus coding EGFP alone, FosB-EGFP or ΔFosB-EGFP was injected into the ventricle. As shown in Figure 11, we found EGFP-positive cells within some limited regions of the ventricle wall 2 days after infection, and mostly only ependymal or subependymal